Novel pathways in cholesterol metabolism to combat cardiometabolic diseases

Zhou, E.

5

Inhibition of Δ24-dehydrocholesterol-reductase activates pro-resolving lipid mediator biosynthesis and inflammation resolution

Andreas Körner, Enchen Zhou, Christoph Müller, Yassene Mohammed, Sandra Herceg, Franz Bracher, Patrick C.N. Rensen, Yanan Wang, Valbona Mirakaj, Martin Giera

Proc Natl Acad Sci U S A 2019 Oct 8;116(41):20623-20634

Abstract

Background

Lipid metabolism is crucial to many (patho-)physiological processes, including inflammation. In particular, cholesterol biosynthesis emerged as an exciting novel therapeutic target in numerous recent studies. Much is known about the early steps in cholesterol biosynthesis, however the later steps have hitherto largely been neglected. We questioned how modifying distal steps in cholesterol biosynthesis could be a possible means for alleviating inflammation.

Methods and results

Using a recently developed chemical probe (SH42) we inhibited distal cholesterol biosynthesis, through selective inhibition of Δ^{24}-dehydrocholesterol reductase (DHCR24). Inhibition of DHCR24 led to an anti-inflammatory/pro-resolving phenotype in a murine peritonitis model. Lipidomics analysis revealed a significant increase in endogenous poly-unsaturated fatty acid (PUFA) biosynthesis. These data integrated with gene expression analysis, revealing increased expression of the desaturase *Fads6* and the key pro-resolving enzyme *Alox-12/15*. Protein array analysis as well as immune cell phenotype and functional analysis substantiated these results confirming the anti-inflammatory/pro-resolving phenotype. Ultimately, lipid mediator analysis revealed the increased production of bioactive lipids, channelling the observed metabolic alterations into a key class of metabolites known for their capacity to change the inflammatory phenotype.

Conclusions

DHCR24 inhibition by SH42 leads to the accumulation of the bioactive metabolite desmosterol, boosting the biosynthesis of PUFA and the downstream production of anti-inflammatory mediators. Our report integrates distal cholesterol biosynthesis and its intermediate desmosterol with endogenous PUFA biosynthesis and resolution of inflammation, rendering this pathway attractive for further developments in the context of pro-resolving therapies.

Introduction

In recent years our knowledge of human lipid metabolism significantly increased, with its role in controlling and defining biological phenotypes in particular. Possibly the most important example is the role of immune cell metabolism in cancer [1]. Consequently, this has triggered scientists to develop novel technologies for studying the interactions between metabolome and phenotype [2]. Moreover, metabolic reprogramming has become accepted as a possible therapeutic strategy [3, 4]. In particular lipid metabolism has long been recognized for its important role in inflammatory processes [5, 6]. However, to date most therapeutic strategies target specific enzymes or receptors, rather than attempting to comprehensively understand and modify lipid metabolism as a key process for the production and homoeostasis of a plethora of lipid derived mediators. In this context we aimed at modifying inflammation through global lipid metabolism changes. We hypothesize that global changes in lipid metabolism can be controlled in such a way that an intrinsically anti-inflammatory/pro-resolving phenotype is observed. We argue that this would require a shift of lipid metabolism towards the increased production of anti-inflammatory and pro-resolving mediators. As particularly n3-PUFA have been described as important precursors of several anti-inflammatory and pro-resolving mediators [7] we therefore questioned how their endogenous production and metabolism could be boosted, especially during an inflammatory event.

Mainly through the recent work of Glass and co-workers [8, 9] we identified Δ^{24}-dehydrocholesterol reductase (DHCR24, also called Seladin-1) as a promising target for controlling lipid metabolism, possibly allowing its reprogramming. DHCR24 is the terminal enzyme in cholesterol biosynthesis, catalysing the transformation of desmosterol to cholesterol (**Figure 1A**). Of the 10 enzymes involved in distal cholesterol biosynthesis, starting with squalene, DHCR24 has recently taken center-stage in several diseases. This enzyme has been linked to Alzheimer's disease (AD), oncogenic and oxidative stress [10], hepatitis C virus (HCV) infections [11], differentiation of Th-17 cells [12], development of foam cells [13] and prostate cancer [14]. While the role of DHCR24 in AD is controversially discussed, it has been postulated as possible drug target for HCV infections [11] as well as arteriosclerosis [8]. Interestingly, this suggests a pronounced involvement of DHCR24 in inflammatory processes as can be further underlined by the actions of its substrate desmosterol. Desmosterol has been shown to interact with the liver X receptors (LXR), the ATP-binding cassette transporter A1 (ABCA1) as well as the sterol response element binding proteins (SREBP) and RORγ [8, 12, 15, 16]. In addition, it has been proven that activation of LXR has a marked influence on immunological functions and PUFA biosynthesis particularly within macrophages (MΦ) [15, 17]. Importantly, PUFA are substrates for the synthesis of immunologically relevant LMs involved in on- and off-set of inflammation[7].

When focusing on LXR as a master regulator of the aforementioned effects, there is no doubt about the possible value of LXR agonists in the context of several diseases [18]. Nevertheless, no LXR agonist has yet reached the clinic. The main drawback of unspecific LXR activators can be attributed to SREBP1c activation, resulting in a severely increased hepatic lipogenesis [19]. This has led researchers to develop specific LXRβ agonists as well as tissue and cell specific drug formulations [18, 20]. In contrast, desmosterol has been described as an LXR agonist and selective interaction partner of SREBP, in that it can likely activate a subset of SREBP1 target genes, despite inhibiting SREBP1 binding to response elements. In turn, DCHR24 integrates cholesterol biosynthesis, LXR activation and inflammation. This raises the question if the endogenous substrate of DHCR24, desmosterol, might be an attractive candidate, fulfilling important requirements for successful LXR activation: i) desmosterol has been shown to bind to LXR in the low micromolar range [16], ii) it possesses a selective

SREBP interaction potential and iii) it inhibits inflammatory gene expression [8]. Recently these processes have been demonstrated in MΦ using desmosterol and desmosterol mimetics [9].

Along these lines we reasoned that inhibition of DHCR24, leading to a controlled desmosterol accumulation, is ideally suited as master regulator of lipid metabolism, allowing to initiate an anti-inflammatory and pro-resolving phenotype. We therefore investigated the metabolic and immunological consequences as well as anti-inflammatory/pro-resolving potential of controlled desmosterol accumulation through selective inhibition of DHCR24 using a recently published, highly *in vivo* active chemical probe (SH42) (K_i 5 nM) [21]. Initially, we evaluated cross reactivity of SH42 with LXR and a set of additional transcription factors; next, we investigated the probes' effects on the course of zymosan A (zyA) induced peritoneal inflammation. Subsequently, lipidomics analysis was carried out in order to understand the observed phenotypic changes on a molecular level. We quantitatively assessed more than 900 lipid species in blood, liver and peritoneal lavage samples. We monitored serum and peritoneal lavage chemokine and gene expression profiles and conducted protein array analysis. Using tandem mass spectrometry analysis, we investigated PUFA levels and the production of specialized pro-resolving and tissue regenerative mediators. Ultimately, we investigated the therapeutic use of SH42 in animal experiments and investigated functional and phenotypic immune cell responses.

Materials and methods

The chemical probe SH42 was prepared as described elsewhere [21]. All animal experiments were approved by the local ethical commission of the Leiden University Medical Center (LUMC), The Netherlands or the Regierungspräsidium Tübingen, Germany. All chemicals were from Sigma Aldrich (St Louis, MO, USA) and of *pro analysi* or LC-MS grade, if not stated otherwise.

Human macrophage differentiation, polarization and lipid analysis

Human PBMCs were isolated from human leukapheresis collars from the Blood Bank of Eberhard-Karls University of Tübingen. For differentiation experiments, cells were either cultured in RPMI 1640 medium alone, with 10 ng/mL human recombinant GM-CSF (Macs Milteny Bergisch Gladbach, Germany), 100 ng/mL M-CSF (Macs Milteny), 0.01 µg/mL desmosterol or 250 µg/mL SH42 at 37°C for 7 days. For polarization experiments, M1 MΦ (monocytes cultured with GM-CSF for 7 days) were stimulated with TNF-α (100 ng/mL; Promokine, Heidelberg, Germany) with and without SH42 (250 µg/mL) or desmosterol (0.01 µg/mL) for 24 hours before transcriptional analysis. For LM analysis 5×10^6 M1 MΦ were stimulated with SH42 (250 µg/mL and/or in combination with zyA (50 µg/mL) for the indicated time points (4 and 24 hours) and quenched with 1.5 mL ice-cold methanol and kept at -80°C until analysis as described below. In an additional set of experiments Baicalein (1 µg/mL) was added together with SH42 and zyA followed by incubation for 24 hours.

LXR selectivity assessment

RAW 264.7 cells were maintained in high glucose Dulbecco's Modified Eagle's (DMEM) with 10% FCS and 1% Penicillin/Streptomycin under 5% CO_2-humidified atmosphere at 37°C. Before treatment, cells were seeded into 24-well plates and incubated for at least 12 hours. Different concentrations of SH42 (dissolved in ethanol) (0, 0.5, 1, 5, 10 µM) were tested and treated cells were incubated for 8h with 10% FCS or 0.5% BSA in DMEM. In the FCS-

starved groups, medium contained 0.5% BSA and 1% Penicillin/Streptomycin DMEM for 8 hours before SH42 treatment. In the Atorvastatin-treated groups, cells were pre-treated with Atorvastatin (dissolved in DMSO) (10/25 μM) for 8 hours before SH42 treatment. Inhibitor experiments with GSK2033 were carried out as follows: cells were treated as described above. In the GSK 2033 treated groups, cells were pretreated with GSK 2033 (5 μM) for 2 hours before SH42 treatment. Cells were ultimately incubated with SH42 (5 μM) with or without pretreatment for 8 h with either 10% FCS or 0.5% BSA in DMEM (No FCS). Control groups were adjusted to 0.1% ethanol and/or DMSO if necessary. RNA was isolated using Tripure RNA Isolation reagent (Roche) according to the manufacturer's protocol. Total RNA (1 μg) was reverse transcribed using Moloney Murine Leukemia Virus (M-MLV) Reverse Transcriptase (Promega) for RT-qPCR according to the manufacturer's instructions to produce cDNA. mRNA expressions were normalized to β-actin and Cyclophilin A mRNA expressions and expressed as fold change compared to vehicle-treated group using the ΔΔCT method. Primer sequences can be found in **supplementary material S11**.

GC-MS analysis of desmosterol levels

Desmosterol levels were determined as described elsewhere with some modifications [21]. For a detailed description of the method, please refer to **supplementary material S12**.

Zymosan A induced peritonitis and FACS analysis

All animal protocols were performed in accordance with the regulations of the Regierungspräsidium Tübingen and the local ethics committee. For all experiments, SH42 was prepared in a 50% sterile Cremophor solution (Merck, Darmstadt, Germany) to a final concentration of 50 μg per μL. Six to eight week old female C57BL/6 mice (Charles River, Sulzfeld, Germany) were injected *i.v.* via the tail vein. Mice were injected daily *i.v*. with SH42 (0.5 mg) or vehicle control in a total volume of 150 μL for a period of three days. The mice were then intraperitoneally (*i.p.*) injected with 1 mL of zyA (1 mg/mL; Sigma-Aldrich, #Z4250). Peritoneal lavages and tissues were obtained at 4, 12, 24 and 48 hours. Collected exudates were washed, suspended in phosphate buffered saline (PBS, Sigma) and counted using a hemocytometer. For differential cell count, cells were blocked with mouse anti-CD16/CD32 (Biolegend, #101320) antibodies for 10 min at room temperature and then stained with anti-mouse e450-F4/80 (eBioscience, #48-4801-82), APC-Ly6G (Biolegend, #127614) and FITC-Ly6C (BioLegend, #128006) antibodies for 30 minutes at 4°C. For determination of MΦ phagocytosis of apoptotic PMNs, cells were permeabilized using a fixation and permeabiliziation kit (BD, #554714) following staining with anti-mouse PerCP-Cy5.5-conjugated anti-Ly6G (Biolegend, #127616) for 30 minutes at 4°C. Data acquisition was performed on a FACSCanto II flow cytometer (BD) using FACSDiva software (BD) and analyzed with FlowJo (TreeStar). The gating strategy can be found in **supplementary material S13** [22]. For therapeutic treatment with SH42, peritonitis was initiated as described above using 1 mL of a zyA solution. A single dose of SH42 was then administered 24 hours later *i.v.* and mice were sacrificed at the 48 hour time-point.

Determination of IL10, IL-6, IL-8, TNF-α and TGFβ

Analysis was carried out according to the manufacturer's instructions using standard ELISA (R&D systems).

Transcriptional analysis of peritoneal cells and macrophages

Human PBMCs were differentiated for 7days in RPMI 1640 supplemented with GM-CSF (10 ng/mL) and then treated with TNF-α (100 ng/mL), SH42 (250 μg/mL) and desmosterol (0.01

μg/mL). Primer sequences can be found in **supplementary material S11**

Peritoneal lavages from SH42 and vehicle treated mice were used following 0 hour and 4 hours of zyA-induced peritonitis prior to transcriptional analysis. Murine 18S expression as a housekeeping gene was evaluated. Primer sequences can be found in **supplementary material S11**.

Protein array analysis

Peritoneal monocytes/MΦ from 3 day SH42 and vehicle treated mice were used following 4 hours of zyA-induced peritonitis. Protein and phosphorylation (TGF-β Phospho Antibody Array, FullMoonBioscience, #PTG176) profiling of peritoneal monocytes (pooled lavages from 5 mice per condition) was performed according to the manufacturer's instructions. Image acquisition was performed by the manufacturer. For a detailed description see **supplementary material S14**.

Human and murine MΦ phagocytosis

Human MΦ were prepared from PBMCs using Histopaque (Sigma Aldrich, St. Louis, USA) method and differentiated with GM-CSF, subsequently 0.1×10^6 cells/well were incubated with test substances as stated. Murine MΦ were obtained by peritoneal lavage and plated on 48-well plates for 1 hour in phosphate buffered saline with calcium and magnesium to allow adherence. Next, MΦ were stimulated with SH42 (250 μg/mL), MaR1 (10 ng/mL) or 19,20 EpDPA (10 ng/mL) as indicated. GSK 2033 was used at a concentration of 200 nM. Fluorescent Zymosan A particles (Thermo Fisher, Cat. No. Z2841) were added at a 1:30 ratio (MΦ:ZyA) and incubated at 37 °C for 60 min to allow phagocytosis. Fluorescence was determined using a fluorescent plate reader (Tecan, Männedorf, Switzerland).

Western Blot analysis

Peritoneal monocytes/MΦ from 3 day SH42 and vehicle treated mice were used following 4 hours of zyA-induced peritonitis. Cell lysates were obtained using RIPA buffer (Cat. 89900, Thermo Fisher Scientific) and determination of protein quantity was performed using standard protocol of Pierce BCA Protein Assay Kit (Cat. 23225, Thermo Fisher Scientific) and protein levels were normalized and loaded in NuPAGE Bis-Tris gels (Thermo Fisher, #NP0335BOX) and blotted on PVDF membranes. Following antibodies were used: anti-mTOR (Cell Signaling Technology, #2972), anti phospho-mTOR (T2446) (abcam, ab63552), anti-pan AKT (abcam, ab8805), anti-phospho-pan AKT (T308) (ab38449) and for loading control an anti-GAPDH antibody (Sigma Aldrich, Cat. G9545). A goat anti-rabbit antibody (ABIN, Cat. 375699) conjugated with alkaline phosphatase (AP) was used as secondary antibody.

Quantitative lipidomics analysis

Quantitative lipdomics analysis was carried out as described elsewhere [23] with some modification. For a detailed description of the method please refer to **supplementary material S15**.

Targeted lipid mediator analysis

Targeted LM analysis was carried out as described elsewhere [22]. For further details please refer to **supplementary material S16**.

Results

The chemical probe SH42 does not interact directly with LXR

To exclude direct LXR activation caused by the employed chemical probe SH42 (**Figure 1**), we investigated the regulation of well-known LXR target genes under treatment with this compound. Since cholesterol biosynthesis in cell culture is only active when extracellular cholesterol is low [24], we treated RAW264.7 MΦ with high concentrations of SH42 in presence and absence of fetal calf serum (FCS) as exogenous source of cholesterol. As can be seen in **Figure 1** the LXR target genes [25] *Abca1* and *Abcg1* (*Srebp1c* only at 5 μM) are only activated when no extracellular cholesterol is available. In turn, SH42 blocks cholesterol biosynthesis [21] and causes LXR activation *via* desmosterol accumulation, but not in a direct fashion; otherwise target gene regulation would also take place when extracellular cholesterol is available. In order to further strengthen this line of argumentation we repeated the incubation of RAW264.7 MΦ with and without FCS under co-treatment with the cholesterol lowering drug Atorvastatin, which interferes with proximal cholesterol biosynthesis. By doing so, the accumulation of steroidal precursors, such as desmosterol, was prevented. As can be seen in **Figure 1** Atorvastatin did block SH42-regulated target gene activation when no extracellular cholesterol (FCS) was present. Again, from these results we conclude that SH42 causes LXR target gene regulation only in conjunction with an activated cholesterol biosynthesis. Hence, not directly interacting with LXR, but via a desmosterol related loop. As an additional line of evidence we repeated the aforementioned experiments in combination with the LXR inverse agonist/antagonist GSK2033 [26]. As can be seen from supplementary material **Figure S1**, treatment with GSK2033 inhibits the expression of LXR target genes e.g. *Abca1* and *Abcg1* mediated by SH42, without affecting *Srebp1c* gene expression. In addition, we monitored possible cross-reactivities with other nuclear receptors, namely, Farnesoid X receptor (FXR), Pregnane X receptor (PXR) and Retinoid X receptor (RXR). We monitored the target gene expression for respectively: *Shp [27]* (FXR)*, Cyp7a1 [28]* (FXR and PXR), *Cyp3a11 [29]* (PXR) and *Cyp27a1 [30, 31]* (PXR and RXR). As can be seen from supplementary material **Figure S1** and **S2**, SH42 did not induce target gene expression of any of these transcription factors. As previously reported, SH42 does pose selective actions on DHCR24 within distal cholesterol biosynthesis [21]. Taken together, these results provide evidence that the actions of SH42 are mediated by a desmosterol related loop without a direct interaction with the here tested transcription factors.

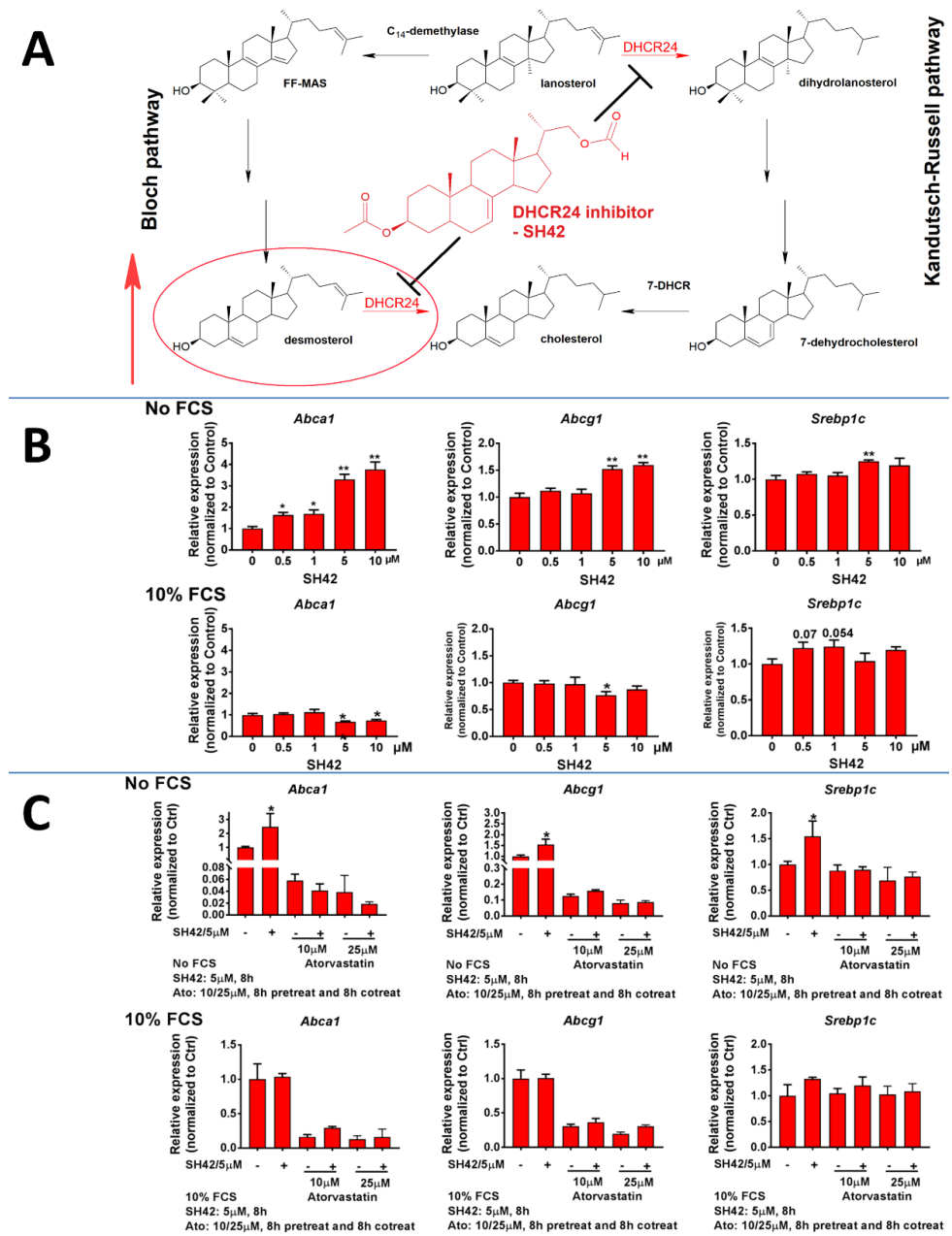

Figure 1 Distal cholesterol biosynthesis, structure of chemical probe SH42 and selectivity assessment. A Structure and action of SH42; the red circle emphasizes desmosterol, accumulating due to blockage of Δ^{24}-dehydrocholesterol reductase (DHCR24). 7-DHCR; 7-dehydrocholesterol reductase. **B** LXR target gene activation (qPCR) with (inactive cholesterol biosynthesis) and without (active cholesterol biosynthesis) fetal calf serum (FCS). **C** LXR target gene regulation under co-treatment with Atorvastatin. All experiments n=5, mean ± SEM, non-parametric student's t-test (Mann-Whitney) comparing each group separately with the control group (no treatment), * $p<0.05$, ** $p<0.01$.

Inhibition of DCHR24 leads to increased inflammation resolution and selectively decreases pro-inflammatory cell influx

Next, we aimed at verifying that inhibition of DHCR24 indeed has a profound effect on acute inflammation. One of the most frequently used animal models for such investigations is the murine zyA induced peritonitis model [32]. Mice were treated once daily (*i.p.*) with 0.5 mg of SH42 for three days, followed by *i.p.* injection of zyA. This was an empirically found dose of SH42 at which we did not observe any acute or long-term toxicity (up to 8 weeks). Desmosterol levels in whole blood, liver and peritoneal exudate were monitored using GC/MS analysis [24]. Blood desmosterol levels proved stable at approximately 5 µg/mL (13 µM) (**Figure 2 A**), while desmosterol was basically absent in the control group. Cellular influx into the peritoneal cavity was monitored using FACS analysis. As can be seen in **Figure 2 B-H,** treatment with SH42 did cause a decrease in leukocyte influx (**panel B**), with a specific decrease in polymorpho-nuclear cells (PMN) ($Ly6G^{hi}$) in the early phase of acute inflammation (**panel C**). To quantify the kinetics of leukocytes, we determined the resolution indices (Ri) [33] displaying a 58% reduction in Ri from 19 hours to 8 hours in mice treated with SH42. This indicated a strong acceleration of inflammation resolution (**panel D**). When focusing on the resolution phase, in which monocytes and MΦ dominate, we found a marked reduction in classical $Ly6C^{hi}$ monocytes (**panel E**), and a significant increase in the non-classical $Ly6C^{lo}$ monocytes (**panel F**) and MΦ (**panel G**) which were accompanied by a significant enhancement in MΦ clearance of apoptotic PMN (**panel H**). Next, we analysed pro- and anti-inflammatory cytokine levels. As can be seen from **panels I-K** pro-inflammatory cytokines were downregulated while anti-inflammatory/pro-resolving cytokines (**panels L/M**) were upregulated. This observation correlated well with the fact that exudate levels of IL-10 and TGF-β, known to be crucial in the resolution of acute inflammation and tissue regeneration, were strongly enhanced (**panel L and M**). Together, these data indicate that SH42 displays an anti-inflammatory, pro-resolving and pro-regenerative impact during acute inflammation. While it has been shown before that activation of LXR in the zyA induced murine peritonitis model alleviates inflammation [34], it is important to note that the chemical probe SH42 does not possess direct LXR activation capacity as detailed above. In turn, the here described effects on cellular influx and population observed in the murine peritonitis model can likely be attributed to a selective inhibition of DHCR24. This is followed by increased levels of desmosterol, which modulates inflammatory outcome by its known actions on LXR [13, 16].

Lipidomic analysis of serum, liver and residential peritoneal cells

Next, we aimed to obtain a better understanding of the underlying molecular factors possibly explaining our findings. In first instance we targeted lipid biosynthesis modulation under treatment with SH42. We furthermore aimed to exclude classic side reactions observed for LXR agonists, such as hypertriglyceridemia and increased lipogenesis [19]. Initially, we monitored liver desmosterol levels, averaging 6.2 ng/mg in the treatment group and 1.9 ng/mg in the control group (**Figure 3A**). Next, we investigated desmosterol levels in the resident peritoneal cell fraction averaging 17.3 versus 1.8 ng/1×10^6 cells in the control group (**Figure 3B**). Using our established GC-MS assay in the scan mode [24] we also screened for other steroidal precursors of cholesterol [35] as well as oxysterols of which neither could be detected under our experimental conditions. Additionally, we found increased blood and serum desmosterol levels under treatment with SH42, as described above and elsewhere [21]. To gain further insights into molecular changes linked to SH42 treatment we carried out comprehensive quantitative lipidomics analysis of serum and liver samples after a 3 day treatment with SH42 (without zyA) [23]. The serum lipid composition showed a significant reduction in the cholesteryl ester (CE) fraction, accompanied by a strong trend towards higher

free fatty acid (FFA) levels (supplementary **Figure S3**). This finding is in-line with SH42 blocking cholesterol biosynthesis leading to lower CE levels. Importantly, no significant increase in the serum triacylglyceride (TAG) fraction was obtained, which is a known side effect of non-selective LXR agonists [19]. When evaluating serum lipid concentrations, we found a significant increase in the FFA concentration with a median of 441 nmol/g in the SH42 versus 363 nmol/g in the control group (**see supplementary Figure S4**). Additionally, we investigated the liver lipidome under treatment with SH42. As can be seen from **Figure S3** a reduced diacylglyceride (DAG) and TAG fraction was observed. This observation was also true for the absolute concentrations for DAG and TAG lipids found per g liver tissue, being 956 and 3718 nmol/g (DAG and TAG) for SH42 treated and 1351 and 6205 nmol/g for control mice, respectively. To gain more mechanistic insights and shed light on the effects of SH42 on the course of zyA-induced peritonitis, we carried out FA compositional analysis of serum, liver and residential peritoneal cells. As LXR has been described to control FA elongation and desaturation [15] we were particularly interested in the FA composition of these lipidomes as we expected to find specific metabolic adaptations under treatment with SH42. As can be seen from **Figure 3 C-E**, we did indeed observe significant changes in the FA composition, mainly in residential peritoneal cells. Our main finding was an increased content of PUFA in the FFA lipid fraction including important precursor FAs for the downstream biosynthesis of specialized pro-resolving mediators (SPM) as, for example, eicosapentaenoic acid (FA20:5) and docosahexaenoic acid (FA22:6). For further details please refer to **Figure 3**.

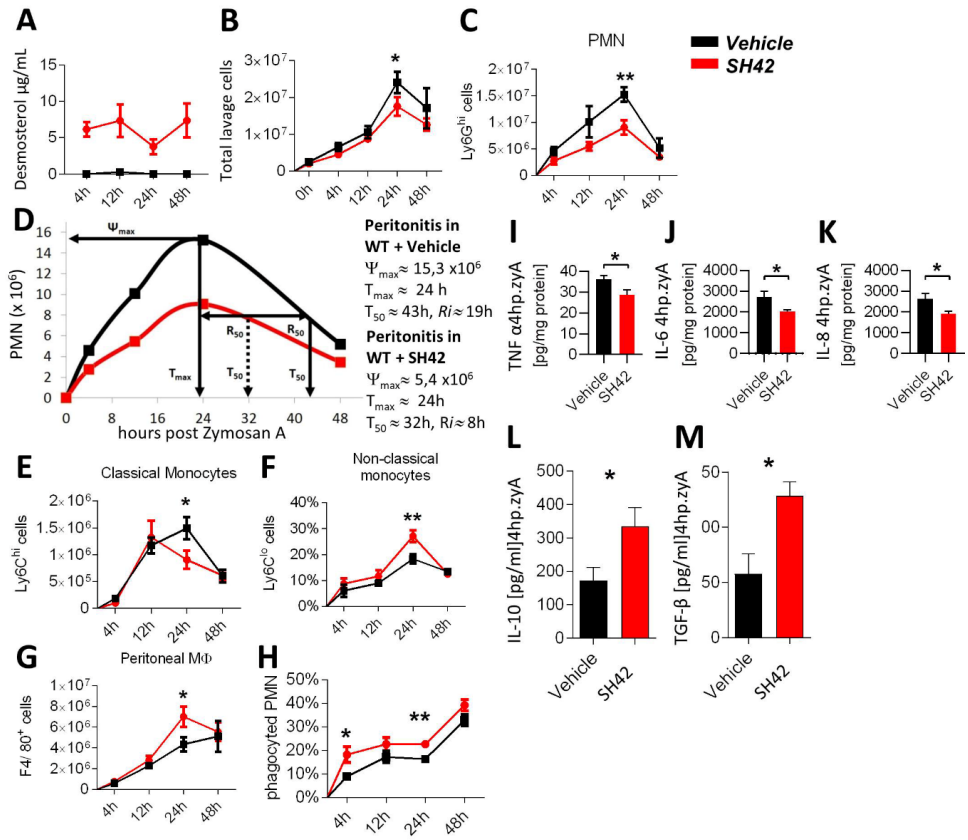

Figure 2 Peritoneal cell analysis. Red lines and circles, SH42 treatment, black lines and squares, vehicle injection. C57BL/6 mice were exposed to zyA-induced peritonitis after three

day treatment with SH42, and peritoneal lavages were collected at 4, 12, 24 and 48 hours. **A** Blood desmosterol levels after the indicated time points (x-axis), **B** The total leukocytes were enumerated by light microscopy, **C** Cell numbers of polymorphonuclear (PMN) Ly6G^{hi} cells, **D** Resolution indices, **E** Cell numbers of classical Ly6C^{hi} monocytes, **F** Cell numbers of non-classical Ly6C^{low} monocytes, **G** Cell numbers of F4/80+ peritoneal MΦ, **H** Cell numbers of monocyte-derived MΦ efferocytosis as analysed by FACS through intracellular staining of PMN, **I**, TNF-α analysis, **J** IL-6 analysis, **K** IL-8 analysis,. **L**, **M** IL-10 and TGF-β levels all measured in the peritoneal fluids (4 hour after zyA). The results represent at least two independent experiments and are expressed as the mean±SEM, n=9-11 per group. All experiments analysed by unpaired student's t-test one per time-point, for desmosterol levels non-paramteric student's t-test (Mann-Whitney) *p<0.05; **p<0.01. For further details please refer to the main text.

Gene expression analysis in liver and peritoneal cells

To substantiate our findings, we next performed gene regulation analysis (qPCR) in liver and peritoneal exudate cells. It has recently been reported that desmosterol and desmosterol mimetics have a cell type specific effect on LXR target gene regulation. Muse et al. showed that desmosterol selectively activates the LXR target gene *ABCA1* (*Abca1*) in MΦ but not in hepatocytes [9]. Along these lines we tested the effects of our chemical probe SH42 *in vivo* in peritoneal lavage cells and liver homogenates. As indicated in supplementary **Figure S5**, the chemical inhibition of DHCR24 decreased expression of *Abca1* alongside *Fasn* without affecting expression of *Scd* in liver homogenates. Gene expression analysis in peritoneal cells focused on *Scd-1, Fads6*, *Elovl1, Elovl5, Elovl6* and *Alox-12/15*. We chose FA desaturase 6 (*Fads6)* because it is one of the rate limiting steps in endogenous PUFA biosynthesis [36]. Further, we monitored *Elovl5* as it is particularly involved in PUFA elongation and *Elovl6* which is an important gene (enzyme) for the elongation of medium to long chain FA [37]. *Alox-12/15* was monitored as an important gene related to PUFA metabolism and in particular the production of SPM. As can be seen from **Figure 4**, when comparing 3-day SH42 treated mice with vehicle control, we observed a trend for an increased expression of *Scd*-1 (p=0.19) as well as a significant increase for *Fads6* expression at time point zero. This finding, together with our lipidomics data (**Figure 3**) pinpointed to an involvement of FA desaturase 6 in increased endogenous PUFA production predominantly in residential peritoneal cells. Our findings are vastly in-line with a previous report on the activation of PUFA biosynthesis mediated by the non-selective LXR agonist T0901317 [15]. Next, we aimed at comparing the changes found in residential peritoneal cells with infiltrating cells during zyA-induced peritonitis. We carried out qPCR analysis of the same genes 4 hours after injecting zyA into the peritoneum. As depicted in **Figure 4** *Fads6* was now down-regulated in the treatment group, while *Elovl-1* and in particular *Alox-12/*15 became up-regulated at the 4 hour time point. Taken together, our data in combination with an earlier report on the activation of PUFA biosynthesis by T0901317 [15] point to increased PUFA biosynthesis mediated by SH42 treatment. Mainly the finding that *Alox-12/15* became up-regulated in the treatment group 4 hours after zyA administration made us interested in a possible link between our initial observations in the zyA-induced self-limiting murine peritonitis model (**Figure 2**) and increased endogenous PUFA production, as well as the possibly altered downstream production of important PUFA metabolites such as eicosanoids and docosanoids.

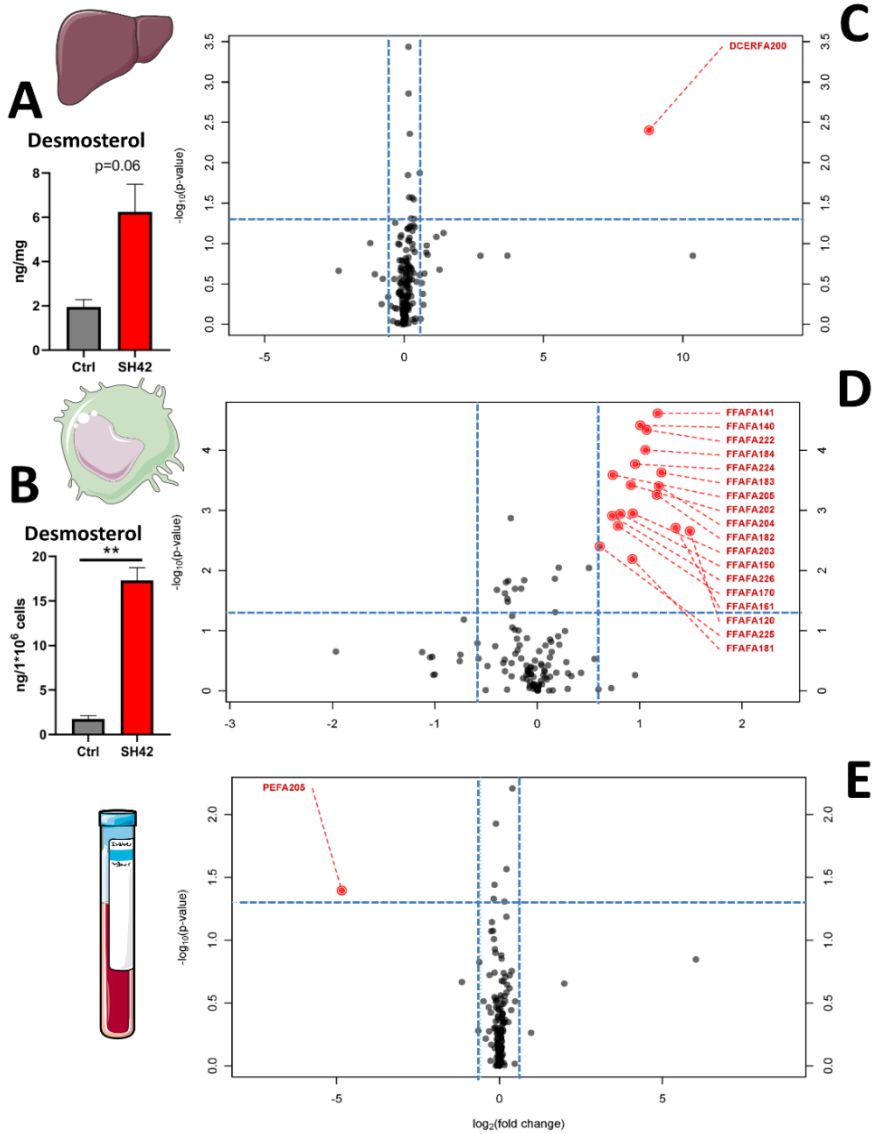

Figure 3 Analysis of the fatty acid composition represented in the different lipidomes and desmosterol after a 3 day treatment with SH42. Panel **A** shows liver desmosterol levels (n=3-5). Panel **B** shows desmosterol amounts found in the residential peritoneal cell fraction (n=4-5). Panels **C-E** volcano plot analysis of the fatty acid composition (FA) of the different lipidomes, each black dot represents a lipid species linked to a specific FA. Lipids are marked red (red dot), when a fold change >1.5 and a p-value < 0.05 was observed, vehicle groups were compared with SH42 treatment. FFA free FA lipid class denoted as FA followed by carbon number and double bond count, e.g. FFAFA204 being free arachidonic acid with 20 carbons and 4 double bonds. Upper panel **C** shows liver lipidomics, middle panel **D** residential peritoneal cell lipidomics and panel **E** serum lipidomics analysis. The blue dotted lines show the fold change and p-value thresholds. The control group was considered as the reference in all comparisons, mean ± SEM, for **A and B** non-parametric student's t-test (Mann-Whitney) ** p<0.01.

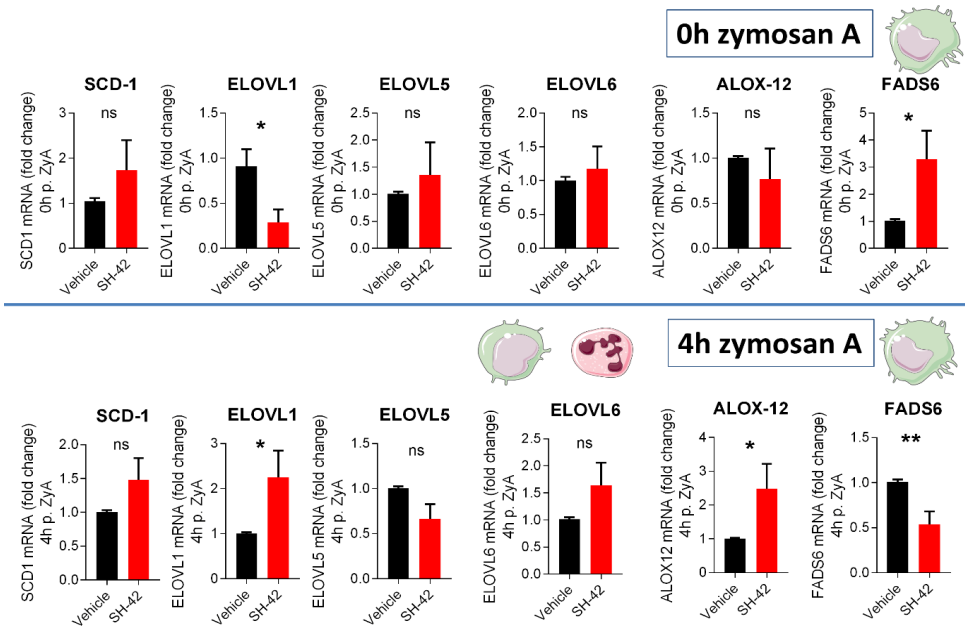

Figure 4 mRNA expression under treatment with SH42. mRNA expression as determined in peritoneal lavage cells from 3 day treated mice versus vehicle at time point 0 hour of zyA induced peritonitis and at time point 4 hours of zyA induced peritonitis. Non-parametric student's t-test (Mann-Whitney), mean ± SEM, * $p<0.05$, ** $p<0.01$, n=10-15.

Inhibition of DHCR24 results in increased biosynthesis of specialized pro-resolving mediators

Based on findings that PUFAs are well-known precursors for the biosynthesis of SPM and other anti-inflammatory lipids [7] and on our own lipidomics and qPCR data obtained from residential peritoneal cells, we questioned whether inhibition of DHCR24 and the here described effects are linked by an increased production of pro-resolving and anti-inflammatory lipids. To investigate this hypothesis we used a standardized liquid chromatography tandem mass spectrometry (LC-MS/MS) approach [38] and profiled peritoneal LM concentrations. As can be seen from **Figure 5** we observed higher PUFA levels particularly at the early 4 hour time point, while other FA such as linoleic and α-linolenic acid (LA and ALA) remained basically unchanged between the treatment and control groups. In front of several recent reports about the immunological function of cytochrome P450 derived epoxy-metabolites, we not only monitored SPM (resolvins), but also 19,20-epoxy docosapentaenoic acid (19,20-EpDPA) and its inactivation product 19,20-dihydroxydocosapentaenoic acid (19,20-diHDPA) [39, 40]. As the here identified mediators are known to actively control inflammation resolution and cellular influx [40], we postulated that their increased biosynthesis under treatment with SH42 might pose a link between LXR activation, increased production of anti-inflammatory and pro-resolving LMs and alleviated inflammatory processes. In this context we also monitored PGE_2 and LTB_4 as established mediators of inflammation (resolution) [41]. As can be seen from **Figure 5L** and supplementary **Figure S6,** PGE_2 was significantly up-regulated in the treatment group, while LTB_4 showed a strong trend ($p=0.06$) towards higher concentrations. For the identification of maresin 1 (MaR1) please refer to the tandem mass spectrometric analysis and

comparison with genuine synthetic standard as provided in supplementary **Figure S7**. The relative retention time (RRT), relative to the internal standard d4-LTB_4, for MaR1 observed in our samples was 0.997 and 0.998 for an authentic standard respectively. In order to substantiate our findings, we carried out a validation experiment at the 4- and 12-hour time points for DHA and its bioactive mediators MaR1 and 19,20-EpDPA. These validation experiments confirmed our findings as can be seen from supplementary **Figure S8.**

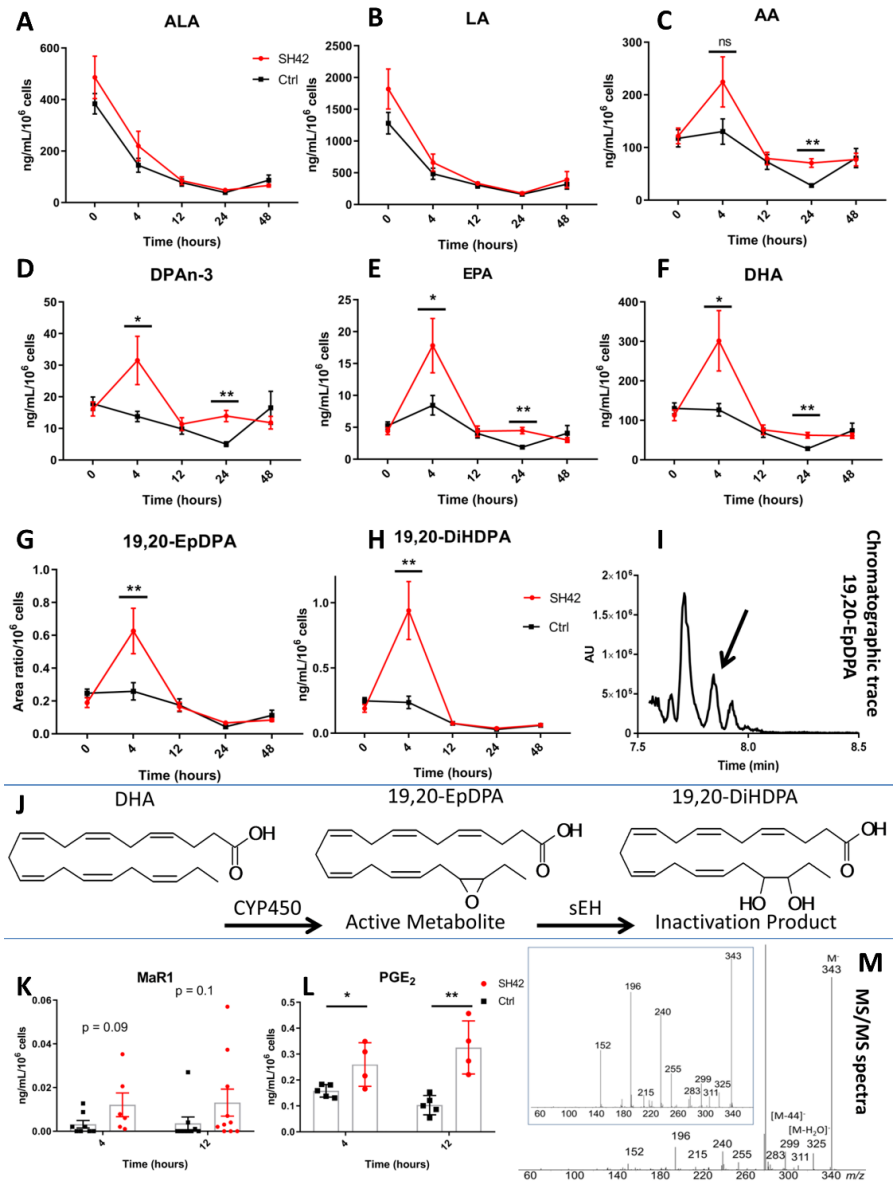

Figure 5 Changes of free FA and the downstream metabolites 19,20-EpDPA and 19,20-DiHDPA in peritoneal lavages in the zyA induced peritonitis model, with and without SH42 treatment. N=6-10 for all experiments, data obtained from two independent experiments with an individual n=3-5 (single experiment for PGE_2 with n=4-5) non-parametric

student's t-test, * p<0.05; ** p<0.01. **A-H**, longitudinal behaviour of various FA during zyA induced peritonitis with and without SH42 treatment (non-parametric student's t-test (Mann-Whitney)). **I** The chromatographic trace showing the transition *m/z* 343 -> 281 was used to detect 19,20-EpDPA. **J** Enzymatic formation of 19,20-EpDPA and 19,20-DiHDPA catalyzed by CYP450 and soluble epoxide hydrolase. **K and L**, levels of MaR1 and PGE_2 observed at the 4 and 12 hour time points (non-parametric students t-test (Mann-Whitney), mean ± SEM, * p<0.05, ** p<0.01). **M**, Tandem mass spectra identifying 19,20-EpDPA compared to an authentic standard (1 ng/mL, blue boxed inlay).

Protein array analysis of the PI3K/AKT and mTOR pathway

In order to expand on these findings and shed more light on the effects of accumulating desmosterol (not cholesterol) under SH42 treatment on the proteomic level we next carried out protein array analysis of residential peritoneal monocytes/MΦ comparing SH42 treatment and vehicle. We focused on the PI3K/AKT and mTOR pathways, as they are crucial in restricting pro-inflammatory responses, thereby promoting anti-inflammatory/pro-resolving responses and activating monocyte/MΦ differentiation and polarization towards a pro-resolving phenotype [42]. To understand if and how SH42 affects these pathways we carried out protein array analysis of peritoneal monocytes after a 3-day treatment with SH42 (**Figure 6**). In the treatment group, marked changes in the expression and phosphorylation of key proteins in both AKT/PI3K and the mTOR pathway were observed. As can be seen from **Figure 6 A,B,** most signalling pathways downstream of AKT did point to anti-inflammatory effects and to changes especially in MΦ survival, cell proliferation, cell growth and gluconeogenesis. In order to substantiate our protein array data, we also carried out western blot analysis of m-TOR and AKT as well as their phosphorylated variants (**Figure 6 C**). Beside these aspects, SH42 regulated the activation of the mTOR pathway and particularly the RICTOR signalling which plays an important role in regulating MΦ metabolism to promote M2 polarization [43]. Notably, the latter observation is in-line with our results observed by lipidomics analysis. This finding was reflected in increased levels of *Alox-12/15* and finally enhanced generation of SPMs, such as Mar1, suggesting that SH42 induces polarization toward the M2 pro-healing and pro-resolving phenotype.

Therapeutic treatment with SH42

Next we questioned whether SH42 would also exert acute besides prophylactic treatment effects. For this we chose the 24 hour time point, resembling the maximum cellular influx after zyA injection (**Figure 2**). Using *in vivo* mouse experiments, we initially monitored blood desmosterol levels after a single (1 day) or repeated (2 days) injection of SH42 in order to investigate whether desmosterol accumulates after a single dose only. This experiment was crucial to correctly interpret the results of the treatment study. If no desmosterol would have accumulated after a single SH42 injection, no causal link could be made between desmosterol and the observed biological phenotype. If so, treatment effects would likely have to be attributed to SH42 itself. As can be seen from **Figure 7** we did indeed observe increased blood desmosterol levels after a single dose of SH42, which further increased after the second dose (without treatment desmosterol is undetectable in blood samples as outlined in **Figure 2A**). Subsequently, we monitored changes in LM biosynthesis and cellular influx at the 48-hour time point. As can be seen from **Figure 7 C and D,** significantly increased concentrations of several PUFA and LM were observed. Additionally, cell numbers and populations were significantly altered in the treatment group (**Figure 7B**), vastly resembling the results of the prophylactic treatment. Taken together, this pinpoints to the fact that SH42 can be used in an

anti-inflammatory therapeutic setting.

Pro-resolving effects and the role of LXR and 12/15-LOX

Ultimately, we aimed at sketching a more functional link between increased desmosterol levels, the increased production of anti-inflammatory lipids and inflammation resolution, as well as give some insight into effects observed in human derived MΦ. To provide these relations we focused our efforts on MΦ phenotype, polarization, phagocytosis, the role of LXR and 12/15-LOX [44] as well as the activation of the CYP, 15-LOX and COX pathways in human MΦ. Phagocytosis (efferocytosis) is a crucial process during inflammation resolution. We initially investigated the effects of SH42 and desmosterol on the phagocytic capacity of human monocyte derived MΦ. As can be seen in **Figure 8,** SH42 was capable of inducing increased phagocytosis starting from approximately 125 µg/mL, while desmosterol showed a positive effect already at doses of no more than 0.01 µg/mL. This points to the fact that desmosterol is the actual mediator of the observed effects (**panels A** and **B**). When co-incubating with the LXR antagonist GSK2033, phagocytosis was blocked and this effect could not be rescued by either SH42 or desmosterol (**panel C**). In turn, this points to a possible role of LXR during this process. To provide additional proof that desmosterol is the actual mediator of SH42s' positive effects, we quantified desmosterol after a 2 hour incubation of human monocyte derived MΦ with high concentrations of SH42. As can be seen from **panel D** we could indeed observe a strong trend towards increased desmosterol concentrations. The other suspected mediators for the described effects of SH42 are MaR1 and 19,20-EpDPA, hence we subsequently investigated the effects of these lipids on MΦ phagocytosis (**panels E and F**). This showed that both lipids positively influenced phagocytosis at low concentrations (10 ng/mL). While 19,20-EpDPA is a cytochrome P450 (CYP) product, MaR1 is biosynthesized by the actions of 12/15-LOX.

To this end we investigated the effects of SH42 on MΦ isolated from either wild-type or 12/15-KO mice, as we had no knock-out model related to the production of 19,20-EpDPA available. As can be seen from **panel G**, treatment of 12/15-LOX KO MΦ did result in diminished phagocytosis. As a next step in integrating our results with inflammation resolution, we focused on monocyte differentiation and MΦ phenotypes as both processes are crucial for inflammation resolution. As cell shape and MΦ phenotype are correlated [45], we carried out cell shape analysis assessing monocyte differentiation towards the M1 or M2 phenotype [22]. As can be seen from **panels H-L** and **M-P**, a 7-day treatment of human derived monocytes (PBMCs) did give a phenotype closely resembling the M-CSF (M2) phenotype. As expected, the effects of desmosterol were significantly lower than observed for SH42, as desmosterol will be further converted into cholesterol if no DCHR24 inhibitor is present (**panels K** and **L-P**). In order to gain more proof that desmosterol and SH42 influence MΦ polarization we assessed mRNA expression markers for both the M1 and M2 phenotype. As can be seen from **panel A and B** in **Figure 9** especially the M2 markers Arg-1 and IL-10 were increased after treatment with both SH42 and desmosterol. Next, as several specific surface receptors are known to play an important role in mediating inflammation resolution [46], we quantified the corresponding mRNA expression and found a significant upregulation of several important receptors (mRNA) (**panel C** in **Figure 9**). In order to further substantiate our functional phagocytosis data we also monitored the expression of well described phagocytic markers [47]. As can be seen from **panel D in Figure 9** we could substantiate our functional phagocytosis data. We observed the increased expression of several phagocytic markers. Ultimately, as we had observed a number of MΦ related functional changes associated with SH42 and desmosterol treatment, we wondered if we could metabolically integrate these finding with the 15-LOX, CYP and cyclooxygenase (COX) pathways. Indeed, when MΦ were treated with zyA with and without

SH42, dramatic metabolic changes could be observed. While zyA-treated MΦ relied mainly on COX driven PUFA metabolism producing high amounts of PGE_2, did co-treatment with SH42 increase not only the intracellular amount of free PUFA but also cause a marked shift towards the CYP and 15-LOX pathway. The latter shows that treatment with SH42 stimulates a metabolic shift towards an anti-inflammatory phenotype as shown by increased levels of the 15-LOX pathway markers 15-HETE (15-hydroxyeicosatetraenoic acid) and 17-HDHA (17-hydroxydocosahexaenoic acid) as well as the CYP-derived LM 19,20-EpDPA (see **Figure 9, panel F**). As validation we repeated the experiment with the LOX inhibitor Baicalein and could block the actions of SH42 (**supplementary material S10**).

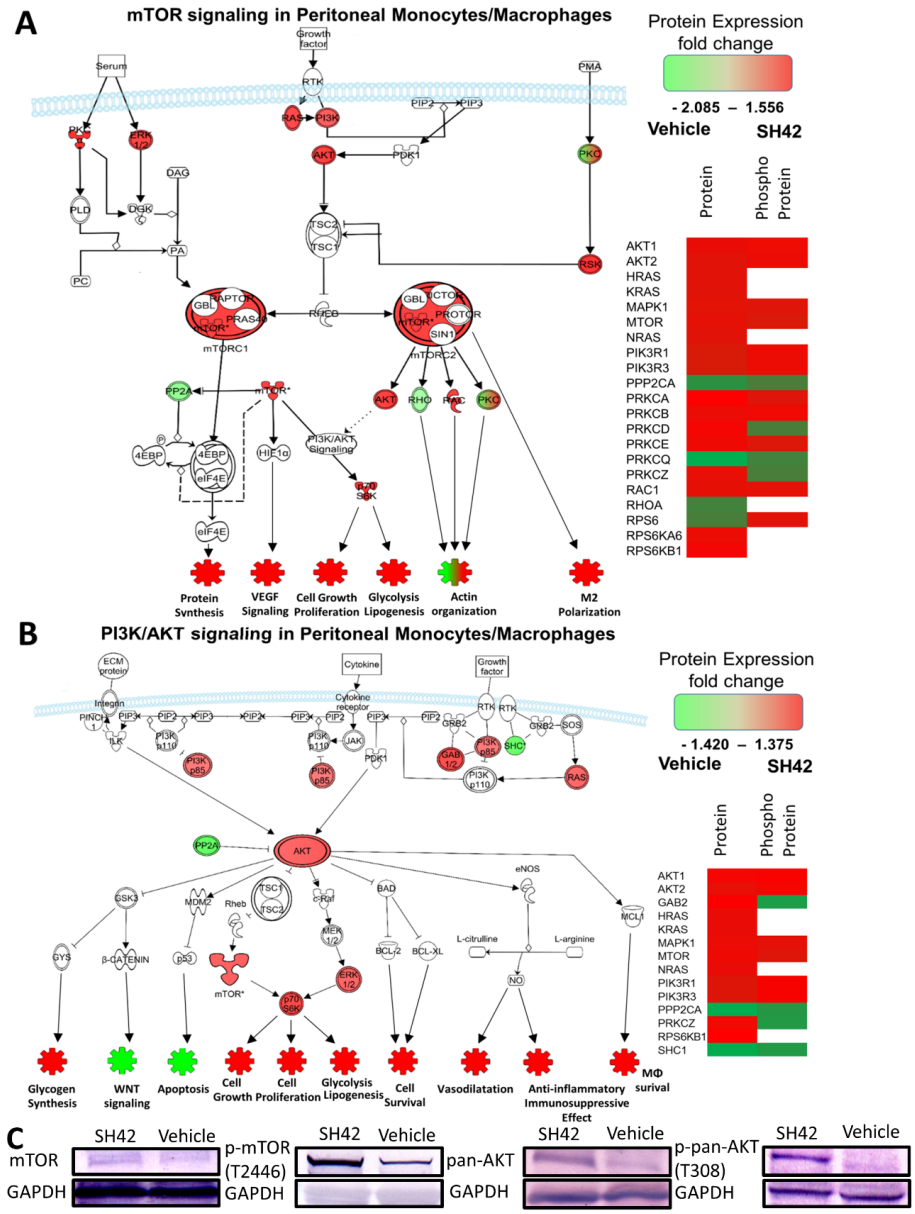

Figure 6 Protein array analysis of the mTOR (A) and PI3K/AKT (B) pathways, the main proteins involved in the mTOR and PI3K/AKT pathway are shown alongside their known physiological functions. Increased protein levels for the SH42 group are shown in red, decreased proteins are shown in green, the corresponding protein fold-changes including phosphoprotein are shown on the right side, **C** Western blot analysis

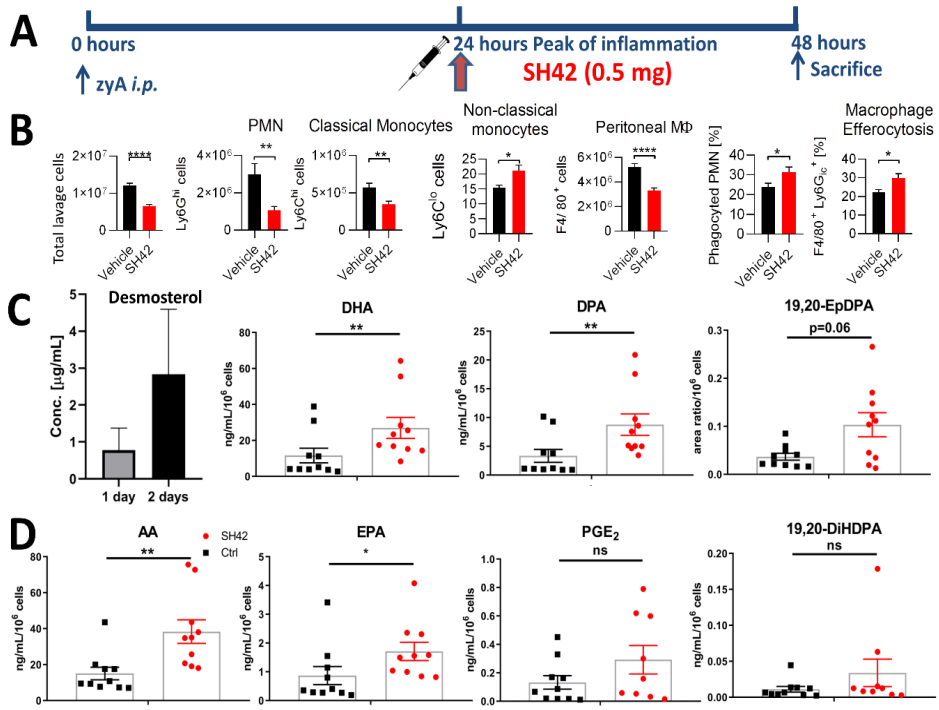

Figure 7 Therapeutic application of SH42. A experimental setup of the SH42 administration, 24 hours after zyA induced inflammation 0.5 mg of SH42 were administered intravenously (*i.v.)* via the tail vein. 24 hours later at the 48 hour time point, mice were sacrificed and peritoneal cells analysed by FACS analysis. **B** FACS results, from left to right, total number of peritoneal lavage cells, PMN, classical monocytes, non-classical monocytes, peritoneal MΦ, percentage of phagocyted PMN, MΦ efferocytosis. **C** and **D** levels of blood desmosterol after a 1 and 2 day treatment followed by PUFA and LM levels in the peritoneal exudates at the 48 hour time point. N=4-5 for desmosterol analyses, n=9-10 for FACS and LM analysis, combined from two individual experiments. Non-parametric student's t-test (Mann-Whitney) for LM and desmosterol analysis, unpaired student's t-test for cellular analysis, mean ± SEM, * $p<0.05$, ** $p<0.01$, **** $p<0.001$

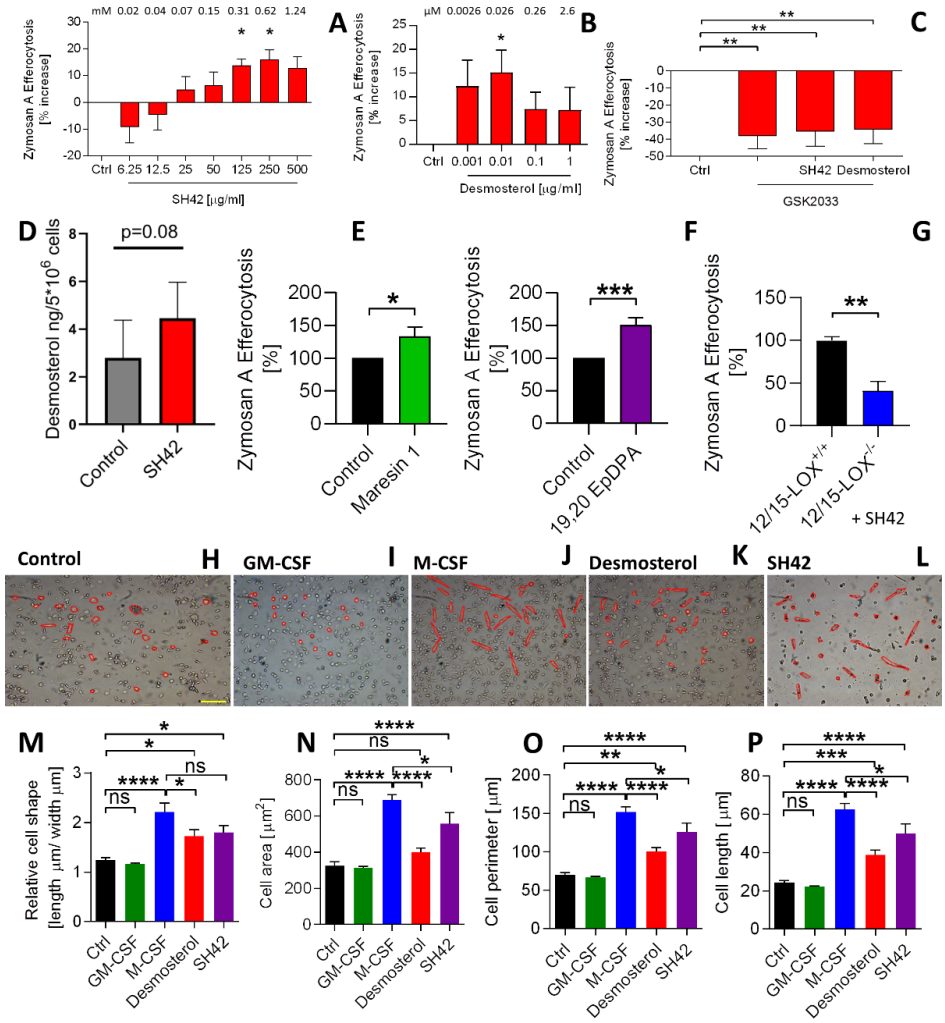

Figure 8 Functional studies of SH42, 19,20-EpDPA and Maresin 1. A phagocytosis under treatment with SH42, **B** phagocytosis with desmosterol treatment, **C** phagocytosis under co-treatment with GSK2033, **A-C**, The results represent at least two independent experiments and are expressed as the mean±SEM, n=9-11 per group, One Way ANOVA with Dunnett's multiple comparison test, **D** desmosterol analysis in SH42 treated MΦ (2 hours), non-parametric student's t-test, **E** phagocytosis with MaR1, phagocytosis with 19,20-EpDPA treatment, **G** phagocytosis comparing WT and 12/15-LOX KO MΦ under treatment (both) with SH42, **E-G** unpaired two-tailed Student's t-test, **H-L** cell shape analysis of human PBMCs stimulated for 7 days with either vehicle (**H**), GMC-SF (**I**), M-CSF (**J**), desmosterol (**K**) or SH42 (**L**), (Scale bar: 100 µm), **M-P** statistical analysis of cell shape, cell area, cell perimeter and cell length, all experiments n=3-11 independent experiments expressed as mean±SEM, **M-P** one-way ANOVA with Bonferroni correction, *p< 0.05; **p< 0.01; ***p<0.001, ****p< 0.0001. Detailed information about the experimental procedures used for cell shape analysis (**H-L**) can be found in the supplementary material **S9.**

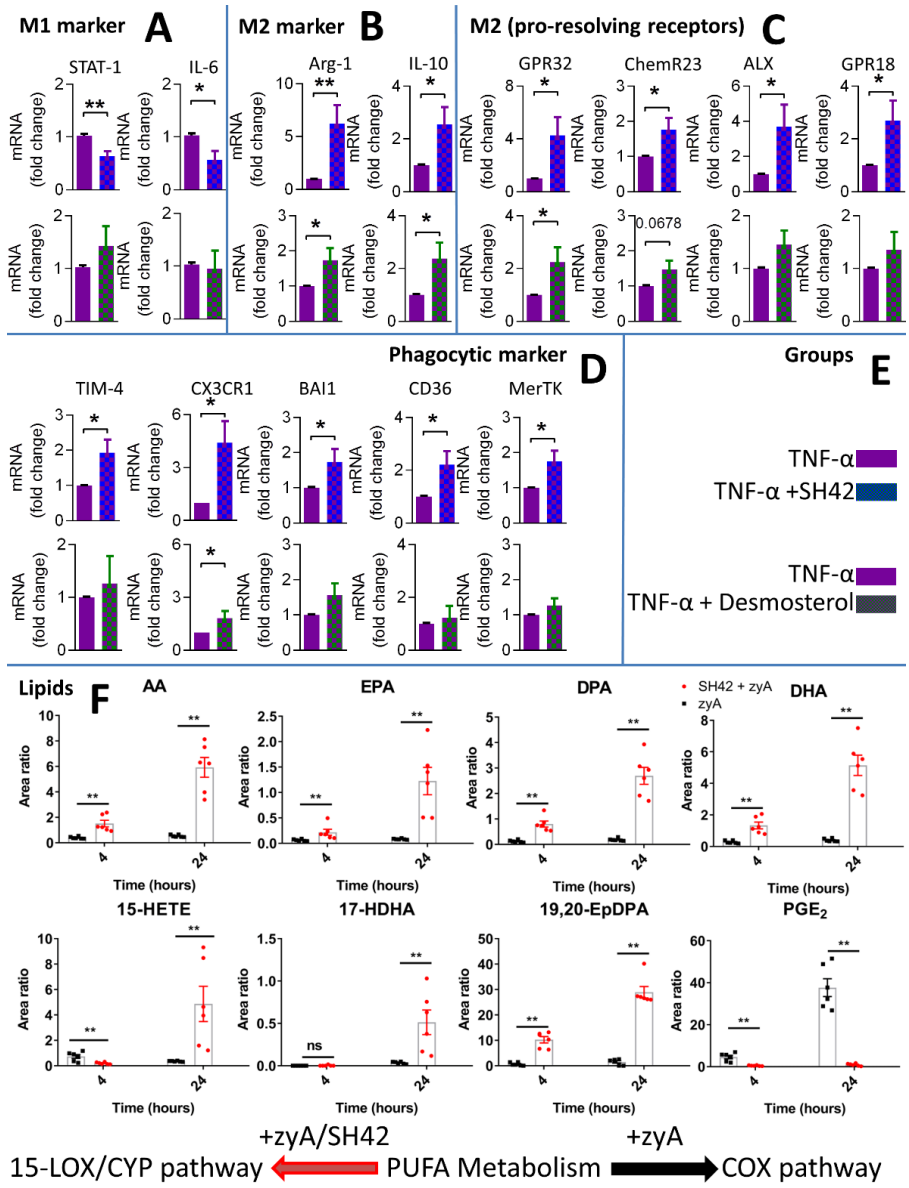

Figure 9 Analysis of MΦ phenotype and PUFA, 15-LOX, CYP and COX pathway markers. M1 **MΦ** were stimulated with TNF-α and in combination with SH42 or desmosterol gene expression was analysed for **panel A** M1 markers, **panel B** M2 markers, **panel C** pro-resolving receptors and **panel D** phagocytic markers, groups are described in **panel E**, all mRNA levels were quantified by RT-PCR (n=9-11). The results are representative of 3–11 independent experiments and are expressed as the mean±SEM, unpaired two-tailed student's t-test, *p< 0.05; **p< 0.01. **Panel F** LC-MS/MS analysis of PUFA, 15-LOX, CYP and COX pathway markers, all experiments n=6 with 3 biological replicates and two technical repeats, non-parametric student's t-test (Mann-Whitney), mean±SEM, ns not significant,**p< 0.01.

Discussion

A summary of the observed effects of SH42 and the here described mechanism of its pro-resolving effect can be found in **Figure 10**.

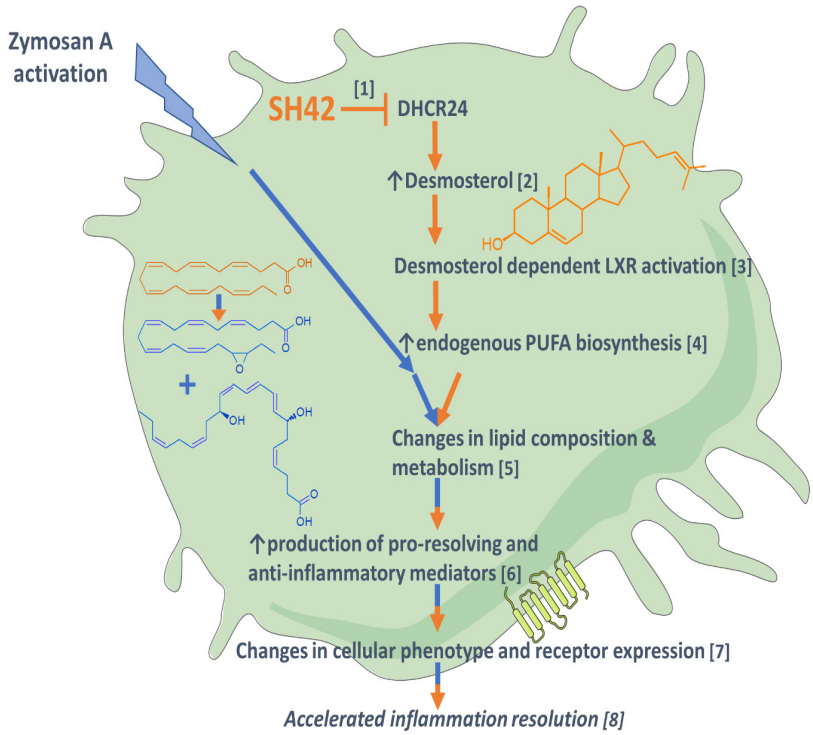

Figure 10 Overview and summary of the observed actions of SH42 in a schematic cell. The effects of SH42 are shown in orange, zyA activation is shown in blue and combined effects in orange/blue **1;** SH42 selectively blocks DHCR24. **2;** inhibition of DHCR24 leads to increased levels of desmosterol. **3;** desmosterol activates LXR. **4;** LXR activation leads to increased endogenous PUFA biosynthesis and **5;** changes in lipid composition and metabolism. **6;** the altered lipidome results in increased production of anti-inflammatory and pro-resolving LM after zyA stimulation. **7;** LMs are known effectors of immune cell phenotype and function, we also observed significant changes in their corresponding receptor expression. **8;** taken together these actions result in accelerated inflammation resolution and modulation.

The fact that DHCR24 has been proposed as potential drug target for several diseases made us interested in the metabolic and immunological role of DHCR24 during inflammation. Using a recently developed highly selective and potent DHCR24 inhibitor (SH42) as a chemical probe [21] we aimed at investigating the consequences of controlled DHCR24 inhibition. In order to separate direct and indirect effects on DHCR24/LXR, it was mandatory to establish the probes' selectivity, allowing for streamlined data interpretation without observing possibly mixed activities. Moreover, we wanted to exclude known side-effects from non-selective LXR activation [19] aiming to exploit the selective functions of desmosterol. We particularly aimed to boost endogenous PUFA biosynthesis and identified desmosterol as a suitable endogenous metabolite mediating such effects. In order to test this hypothesis we initially investigated the probe's influence on the course of zyA-induced peritonitis [32]. SH42 did have a marked

influence on relevant numbers and types of inflammation related immune cells. Particularly anti-inflammatory/tissue regenerative cell types were found up-regulated upon treatment with SH42. In line with these findings increased levels of IL-10, TGFβ and increased efferocytotic capacity were found. In order to shed some light on the underlying molecular mechanisms we carried out quantitative lipidomic analysis.

Monitoring almost 1000 individual lipid species, we observed increased amounts of longer chain FA as well as increased PUFA content. This change in lipid metabolism, which was mainly observed in residential peritoneal cells, proved that our hypothesis of boosting PUFA biosynthesis through the controlled accumulation of desmosterol is possible. As SPM are well known and characterized downstream products of PUFA [7] we rationalized that altered lipid metabolism, leading to increased endogenous PUFA production, might ultimately lead to changed LM profiles during on- and off-set of inflammation. Indeed, we found a significant increase in the gene expression of the desaturase *Fads6* in residential peritoneal cells (**Figure 4**) from mice treated with SH42. After inducing inflammation, a significant difference between vehicle and SH42 treatment in the expression of the key pro-resolving enzyme *Alox-12/15* was observed. This result clearly pinpointed to a molecular modulation of the course of murine peritoneal inflammation. The increased expression of *Alox-12/15* found in the peritoneal cavity might reflect an altered reaction to zyA stimulation, mediated through Toll-like receptor (TLR) stimulation. Ito et al. [48] showed that LXR controls a plethora of genes involved in lipid metabolism, this function correlates with its ability to modulate membrane lipid organization and thereby influence TLR signalling [18, 25]. A direct link between LXR and *Alox-12/15* has been laid particularly in human M2 MΦ [49]. However, to our knowledge no report has yet pointed out an LXR dependent increase in the expression of peritoneal *Alox-12/15*. Nevertheless, it seems conceivable that changes in lipid metabolism, caused by desmosterol driven LXR activation, might ultimately translate into a differential response to zyA stimulation. This might explain altered gene expression profiles at the early 4 hour time point.

Having observed these marked changes in lipid metabolism and gene expression of related enzymes we next investigated PUFA metabolism. Using a standardized LC-MS/MS platform we analysed peritoneal LM profiles under treatment with SH42 during murine peritonitis. As can be seen from **Figure 5** we observed increased free PUFA levels in mice under treatment with SH42 at the 4 hour time point, this finding correlated well with our lipidomic results. Likely the increased levels of PUFA stem from the altered lipid metabolism/composition of the residential MΦ as described by lipidomic and gene expression analysis. Additionally, increased levels of the well-established eicosanoids LTB_4 and PGE_2 as well as the pro-resolving docosanoid MaR1 and the epoxy metabolite 19,20-EpDPA and its inactive metabolite 19,20-DiHDPA were observed. LTB_4 levels were enhanced at the 4 hour time point in the treatment group, with a rapid decrease towards the 12 hour time point. The levels of PGE_2 remained elevated at 12 hours in the treatment group. Although this finding might initially seem counter-intuitive it is important to realize that PGE_2 has been described as important mediator of LM class switching in the early phase of inflammatory processes [41]. Moreover, several recent reports have underlined possible anti-inflammatory effects exerted by PGE_2 [50]. In turn, the increased levels of PGE_2 found at 4 and 12 hours are likely contributing to the observed effects of SH42. Additionally, the increased production of MaR1 was in-line with the altered gene expression of *Alox-12/15*, a key enzyme necessary for the biosynthesis of anti-inflammatory/pro-resolving mediators. With respect to the involved receptors, to our knowledge no definite receptor has yet been identified for 19,20-EpDPA [51]. However, MaR1 has been shown to be a partial agonist of recombinant human BLT1 receptor, likely

antagonizing the actions of the pro-inflammatory mediator LTB_4 [52]. Kd values for several pro-resolving LMs are described to be in the pico- to nanomolar range [53], a concentration range which can possibly be reached in our model. Along this line we argued that *Alox-12/15* derived LMs as well as the increased concentrations of epoxy-metabolites (*i.e.* 19,20-EpDPA) are the final downstream products possibly explaining the actions of SH42 [39].

In order to gain more insight on the proteomic level we carried out protein array analysis of the AKT/PI3K and mTOR pathways (**Figure 6**) in residential peritoneal cells. Also, on the proteomic level we found a significant skewing towards a more anti-inflammatory phenotype. Interestingly, these results pinpoint to an intertwined change of lipidome and proteome, jointly changing metabolism and actions of peritoneal monocytes, thereby mediating the actions of SH42. It seems plausible that these observations are mediated by changes in lipid metabolism and possibly lipid rafts, altering cellular signalling. Integration of LXR and AKT signalling mediated by changes in lipid rafts have been described in cancer cells [54]. However, to our knowledge the control of AKT/PI3K and mTOR in a DHCR24/LXR dependent fashion has not yet been shown.

Next, we tested if SH42 would also prove beneficial in a therapeutic setting and carried out additional mouse experiments in order to gain more mechanistic and functional insights into the relation between desmosterol, LXR and the observed anti-inflammatory effects. As can be seen from **Figure 7** SH42 did also give rise to anti-inflammatory effects when administered at the peak of inflammation (24-hour time point). It was important to see that already after a single dose of SH42 we could observe the accumulation of desmosterol, as otherwise possible anti-inflammatory effects would have had to be attributed to SH42 itself. Nevertheless, it is important to stress that we cannot entirely exclude other biological effects related to SH42, beyond inhibiting DHCR24. Finally, we investigated the mechanistic relationship between SH42, desmosterol, MaR1, 19,20-EpDPA, LXR and ALOX-12/15. For this we chose monocyte differentiation and polarization as well as MΦ phagocytosis as functional read outs, two important hallmarks of inflammation resolution. As can be seen from **Figure 8**, MaR1, 19,20-EpDPA, SH42 and desmosterol were capable of inducing the pro-resolving M2 MΦ type, as well as enhancing phagocytosis. Much higher doses of SH42 were needed when compared to desmosterol, MaR1 and 19,20-EpDPA. This speaks for the fact that desmosterol as well as MaR1 and 19,20-EpDPA are the actual mediators of the effects observed under SH42 treatment. We substantiated our findings by gene expression analysis showing a shift towards the pro-healing MΦ phenotype (**Figure 9**). Additionally, our functional findings were accompanied by an increased expression of several important pro-resolving receptors (GPR32, ChemR23, ALX and GPR18), strengthening our line of argumentation. These receptors have just recently been shown to be involved in inflammation resolution in a human skin blister model [55]. Ultimately, we monitored important CYP, 15-LOX and COX pathway markers under treatment of human MΦ with zyA, with and without SH42. We found a dramatic shift towards the 15-LOX and CYP pathway under co-treatment with SH42 (**Figure 9**). MΦ only stimulated with zyA almost solely relied on COX metabolism, producing large amounts of PGE_2. The aforementioned findings might open novel treatment opportunities, as polymorphisms in the 15-LOX pathway have been linked with the development of asthma, arthritis and atherosclerosis in humans. Products of this pathway (MaR1 and LXA_4) have been described in a human skin blister model [55, 56].

In summary (**Figure 10**), we here describe the anti-inflammatory effects of SH42 as a highly potent and selective inhibitor of DHCR24. SH42 leads to an accumulation of desmosterol, subsequently activating LXR and affecting PUFA metabolism mainly in residential monocytes. These changes are down-stream translated into the increased production of pro-resolving

mediators, likely mediating the observed effects. In turn, targeting lipid metabolism at a presumably distinct point (such as cholesterol biosynthesis) can have profound effects on the general lipid composition with fundamental consequences for cellular phenotypes and inflammatory outcome. Endogenous n3-PUFA production has long been considered neglectable when compared to dietary sources. It has been established that humans almost entirely depend on the dietary uptake of n3-PUFA and the possibility of boosting endogenous n3-PUFA biosynthesis to target crucial physiological processes such as inflammation-resolution is vastly unexplored. However, our here presented data strongly indicate that interfering with lipid metabolism at an appropriate junction can trigger endogenous PUFA biosynthesis and the downstream production of pro-resolving lipids which, in turn, translates into important functional and phenotypic changes. We are confident that our study can form the fundament for a better understanding of the interplay between cholesterol biosynthesis, LXR and the production of pro-resolving lipids, possibly posing a novel means for targeting inflammatory diseases.

Acknowledgements

We thank Shane Soogea, Evelyne Steenvoorden, and Marieke Heijink for their help with lipid analysis. We thank Marije Kuipers for help with the artwork of Fig. 10. This work was supported by 2 grants from the Deutsche Forschungsgemeinschaft (DFG; German Research Foundation): DFG-MI 1506/5-1 and Projektnummer 374031971–TRR 240 (to V.M.); and IZKF-Fortüne Grant 2377-0-0 (to A.K.). This research was also supported by the Enabling Technologies Hotels Programme-ZonMW Grant 4350004007 (to Y.W. and M.G.). Y.W. is supported by VENI Grant 91617027 from the Netherlands Organization for Scientific Research-ZonMW. M.G. is supported by and coordinator of the Horizon2020 Innovative Training Network (ITN) project, ArthritisHeal 812890. E.Z. is supported by the China Scholarship Council (CSC, grant 201606010321).

Author contributions

P.C.N.R., Y.W., V.M., and M.G. designed research; A.K., E.Z., C.M., and M.G. performed research; S.H., F.B., and M.G. contributed new reagents/analytic tools; A.K., E.Z., C.M., Y.M., P.C.N.R., Y.W., V.M., and M.G. analyzed data; A.K., E.Z., C.M., Y.M., F.B., P.C.N.R., Y.W., V.M., and M.G. wrote the paper; V.M. contributed to study design; and M.G. guided overall study design.

Conflict of interest

The authors report no declarations of interest.

References

1. Pavlova, Natalya N. and Craig B. Thompson, *The Emerging Hallmarks of Cancer Metabolism.* Cell Metabolism, 2016. **23**(1): p. 27-47.
2. Rinschen, M.M., et al., *Identification of bioactive metabolites using activity metabolomics.* Nature Reviews Molecular Cell Biology, 2019.
3. Luengo, A., D.Y. Gui, and M.G. Vander Heiden, *Targeting Metabolism for Cancer Therapy.* Cell Chemical Biology, 2017. **24**(9): p. 1161-1180.
4. Hiebert, P. and S. Werner, *Targeting metabolism to treat psoriasis.* Nature Medicine, 2018. **24**(5): p. 537-539.
5. Serhan, C.N., *Discovery of specialized pro-resolving mediators marks the dawn of resolution physiology and pharmacology.* Molecular Aspects of Medicine, 2017. **58**: p. 1-11.
6. van Diepen, J.A., et al., *Interactions between inflammation and lipid metabolism: Relevance for efficacy of anti-inflammatory drugs in the treatment of atherosclerosis.* Atherosclerosis, 2013. **228**(2): p. 306-315.
7. Serhan, C.N. and N.A. Petasis, *Resolvins and Protectins in Inflammation Resolution.* Chemical Reviews, 2011. **111**(10): p. 5922-5943.
8. Spann, N.J. and C.K. Glass, *Sterols and oxysterols in immune cell function.* Nat Immunol, 2013. **14**(9): p. 893-900.
9. Muse, E.D., et al., *Cell-specific discrimination of desmosterol and desmosterol mimetics confers selective regulation of LXR and SREBP in macrophages.* Proceedings of the National Academy of Sciences, 2018. **115**(20): p. E4680-E4689.
10. Wu, C., et al., *Regulation of cellular response to oncogenic and oxidative stress by Seladin-1.* Nature, 2004. **432**(7017): p. 640-645.
11. Takano, T., et al., *Augmentation of DHCR24 expression by hepatitis C virus infection facilitates viral replication in hepatocytes.* Journal of Hepatology, 2011. **55**(3): p. 512-521.
12. Cederbaum, A.I., *Molecular mechanisms of the microsomal mixed function oxidases and biological and pathological implications.* Redox Biology, 2015. **4**(Supplement C): p. 60-73.
13. Spann, Nathanael J., et al., *Regulated Accumulation of Desmosterol Integrates Macrophage Lipid Metabolism and Inflammatory Responses.* Cell, 2012. **151**(1): p. 138-152.
14. Guo, H., et al., *Modulation of long noncoding RNAs by risk SNPs underlying genetic predispositions to prostate cancer.* Nat Genet, 2016. **48**(10): p. 1142-1150.
15. Varin, A., et al., *Liver X Receptor Activation Promotes Polyunsaturated Fatty Acid Synthesis in Macrophages.* Arteriosclerosis, Thrombosis, and Vascular Biology, 2015. **35**(6): p. 1357.
16. Yang, C., et al., *Sterol Intermediates from Cholesterol Biosynthetic Pathway as Liver X Receptor Ligands.* Journal of Biological Chemistry, 2006. **281**(38): p. 27816-27826.
17. Oishi, Y., et al., *SREBP1 Contributes to Resolution of Pro-inflammatory TLR4 Signaling by Reprogramming Fatty Acid Metabolism.* Cell Metabolism, 2017. **25**(2): p. 412-427.
18. Hong, C. and P. Tontonoz, *Liver X receptors in lipid metabolism: opportunities for drug discovery.* Nat Rev Drug Discov, 2014. **13**(6): p. 433-444.
19. Schultz, J.R., et al., *Role of LXRs in control of lipogenesis.* Genes & Development, 2000. **14**(22): p. 2831-2838.
20. Gadde, S., et al., *Development of Therapeutic Polymeric Nanoparticles for the*

Resolution of Inflammation. Advanced Healthcare Materials, 2014. **3**(9): p. 1448-1456.
21. Müller, C., et al., *New chemotype of selective and potent inhibitors of human delta 24-dehydrocholesterol reductase.* European Journal of Medicinal Chemistry, 2017. **140**: p. 305-320.
22. Körner, A., et al., *Sympathetic nervous system controls resolution of inflammation via regulation of repulsive guidance molecule A.* Nature Communications, 2019. **10**(1): p. 633.
23. Ubhi, B.K., *Direct Infusion-Tandem Mass Spectrometry (DI-MS/MS) Analysis of Complex Lipids in Human Plasma and Serum Using the Lipidyzer™ Platform*, in *Clinical Metabolomics: Methods and Protocols*, M. Giera, Editor. 2018, Springer New York: New York, NY. p. 227-236.
24. Giera, M., F. Plössl, and F. Bracher, *Fast and easy in vitro screening assay for cholesterol biosynthesis inhibitors in the post-squalene pathway.* Steroids, 2007. **72**(8): p. 633-642.
25. Calkin, A.C. and P. Tontonoz, *Transcriptional integration of metabolism by the nuclear sterol-activated receptors LXR and FXR.* Nature Reviews Molecular Cell Biology, 2012. **13**: p. 213.
26. Zuercher, W.J., et al., *Discovery of Tertiary Sulfonamides as Potent Liver X Receptor Antagonists.* Journal of Medicinal Chemistry, 2010. **53**(8): p. 3412-3416.
27. Jiao, Y., Y. Lu, and X.-y. Li, *Farnesoid X receptor: a master regulator of hepatic triglyceride and glucose homeostasis.* Acta Pharmacologica Sinica, 2014. **36**: p. 44.
28. Chiang, J.Y.L., *Regulation of bile acid synthesis: pathways, nuclear receptors, and mechanisms.* Journal of Hepatology, 2004. **40**(3): p. 539-551.
29. Zhou, J., et al., *A Novel Pregnane X Receptor-mediated and Sterol Regulatory Element-binding Protein-independent Lipogenic Pathway.* Journal of Biological Chemistry, 2006. **281**(21): p. 15013-15020.
30. Li, T., W. Chen, and J.Y.L. Chiang, *PXR induces CYP27A1 and regulates cholesterol metabolism in the intestine.* Journal of Lipid Research, 2007. **48**(2): p. 373-384.
31. QUINN, Carmel M., et al., *Expression and regulation of sterol 27-hydroxylase (CYP27A1) in human macrophages: a role for RXR and PPARγ ligands.* Biochemical Journal, 2005. **385**(3): p. 823-830.
32. Cash, J.L., G.E. White, and D.R. Greaves, *Chapter 17 ZymosanA Induced Peritonitis as a Simple Experimental System for the Study of Inflammation*, in *Methods in Enzymology*. 2009, Academic Press. p. 379-396.
33. Serhan, C.N. and B.D. Levy, *Resolvins in inflammation: emergence of the pro-resolving superfamily of mediators.* The Journal of Clinical Investigation, 2018. **128**(7): p. 2657-2669.
34. Choi, J.-Y., et al., *Mer signaling increases the abundance of the transcription factor LXR to promote the resolution of acute sterile inflammation.* Science Signaling, 2015. **8**(365): p. ra21-ra21.
35. Mailänder-Sánchez, D., et al., *Antifungal defense of probiotic Lactobacillus rhamnosus GG is mediated by blocking adhesion and nutrient depletion.* PLOS ONE, 2017. **12**(10): p. e0184438.
36. He, C., et al., *Inhibiting Delta-6 Desaturase Activity Suppresses Tumor Growth in Mice.* PLoS ONE, 2012. **7**(10): p. e47567.
37. Matsuzaka, T. and H. Shimano, *Elovl6: a new player in fatty acid metabolism and insulin sensitivity.* Journal of Molecular Medicine, 2009. **87**(4): p. 379-384.
38. Schlegel, M., et al., *The neuroimmune guidance cue netrin-1 controls resolution*

programs and promotes liver regeneration. Hepatology, 2016. **63**(5): p. 1689-1705.
39. Shimanaka, Y., et al., *Omega-3 fatty acid epoxides are autocrine mediators that control the magnitude of IgE-mediated mast cell activation.* Nature Medicine, 2017. **23**: p. 1287.
40. Gilroy, D.W., et al., *CYP450-derived oxylipins mediate inflammatory resolution.* Proceedings of the National Academy of Sciences, 2016. **113**(23): p. E3240-E3249.
41. Levy, B.D., et al., *Lipid mediator class switching during acute inflammation: signals in resolution.* Nature Immunology, 2001. **2**: p. 612.
42. Manning, B.D. and A. Toker, *AKT/PKB Signaling: Navigating the Network.* Cell, 2017. **169**(3): p. 381-405.
43. Covarrubias, A.J., et al., *Akt-mTORC1 signaling regulates Acly to integrate metabolic input to control of macrophage activation.* eLife, 2016. **5**: p. e11612.
44. Greenlee-Wacker, M.C., *Clearance of apoptotic neutrophils and resolution of inflammation.* Immunological Reviews, 2016. **273**(1): p. 357-370.
45. McWhorter, F.Y., et al., *Modulation of macrophage phenotype by cell shape.* Proceedings of the National Academy of Sciences, 2013. **110**(43): p. 17253-17258.
46. Buckley, Christopher D., Derek W. Gilroy, and Charles N. Serhan, *Proresolving Lipid Mediators and Mechanisms in the Resolution of Acute Inflammation.* Immunity, 2014. **40**(3): p. 315-327.
47. Gordon, S., *Phagocytosis: An Immunobiologic Process.* Immunity, 2016. **44**(3): p. 463-475.
48. Ito, A., et al., *LXRs link metabolism to inflammation through Abca1-dependent regulation of membrane composition and TLR signaling.* eLife, 2015. **4**: p. e08009.
49. Huang, J.T., et al., *Interleukin-4-dependent production of PPAR-γ ligands in macrophages by 12/15-lipoxygenase.* Nature, 1999. **400**: p. 378.
50. FitzGerald, G.A., *Bringing PGE₂ in from the cold.* 2015. **348**(6240): p. 1208-1209.
51. Bishop-Bailey, D., et al., *Lipid-Metabolizing CYPs in the Regulation and Dysregulation of Metabolism.* 2014. **34**(1): p. 261-279.
52. Colas, R.A., et al., *Identification and Actions of the Maresin 1 Metabolome in Infectious Inflammation.* 2016. **197**(11): p. 4444-4452.
53. Spite, M., J. Clària, and Charles N. Serhan, *Resolvins, Specialized Proresolving Lipid Mediators, and Their Potential Roles in Metabolic Diseases.* Cell Metabolism, 2014. **19**(1): p. 21-36.
54. Pommier, A.J.C., et al., *Liver X Receptor activation downregulates AKT survival signaling in lipid rafts and induces apoptosis of prostate cancer cells.* Oncogene, 2010. **29**: p. 2712.
55. Motwani, M.P., et al., *Pro-resolving mediators promote resolution in a human skin model of UV-killed Escherichia coli–driven acute inflammation.* JCI Insight, 2018. **3**(6).
56. Wittwer, J., J. Marti-Jaun, and M. Hersberger, *Functional polymorphism in ALOX15 results in increased allele-specific transcription in macrophages through binding of the transcription factor SPI1.* Human Mutation, 2006. **27**(1): p. 78-87.

Supplemental appendix

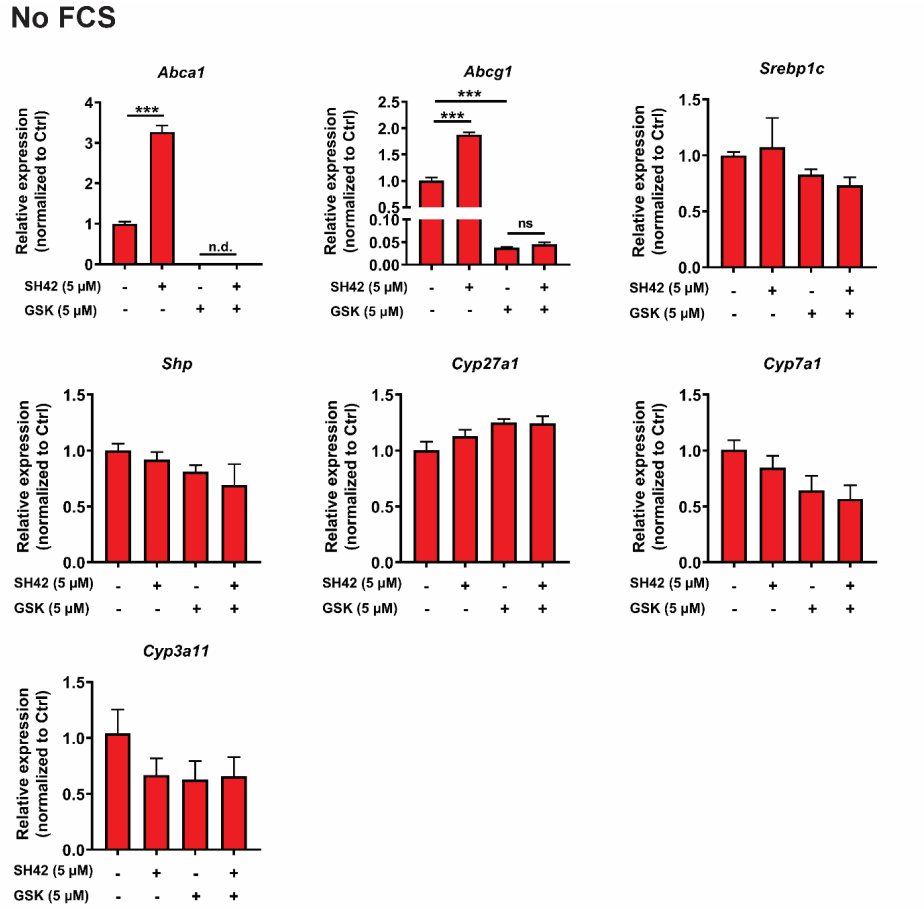

S1. qPCR analysis of SH42/GSK2033 co-treatment and evaluation of additional transcription factor target genes without FCS being present (=active distal cholesterol biosynthesis). n.d. not detected. Mean±SEM, non-parametric students t-test (Mann-Whitney, one per conditions against control). Inhibitor experiments with GSK2033 were carried out as follows: In the GSK 2033 treated groups, cells were pretreated with GSK 2033 (5 µM) for 2 hours before SH42 treatment. Cells were ultimately incubated with SH42 (5 µM). RNA was isolated using Tripure RNA Isolation reagent (Roche) according to the manufacturer's protocol. Total RNA (1 µg) was reverse transcribed using Moloney Murine Leukemia Virus (M-MLV) Reverse Transcriptase (Promega) for RT-qPCR according to the manufacturer's instructions to produce cDNA. mRNA expressions were normalized to β-actin and Cyclophilin A mRNA expressions and expressed as fold change compared to vehicle-treated groups using the ΔΔCT method. Primer sequences can be found in **supplementary material S11**. For further details please refer to the materials and methods section.

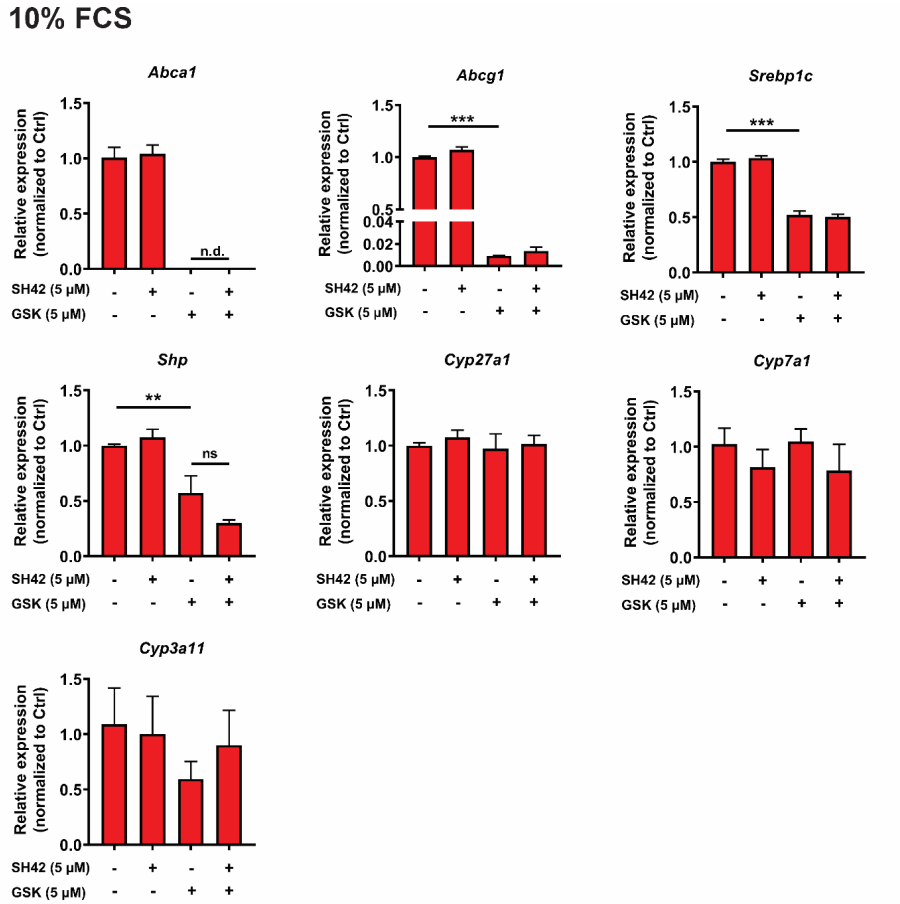

S2. qPCR analysis of SH42/GSK2033 co-treatment and evaluation of additional transcription factor target genes with FCS being present (=inactive distal cholesterol biosynthesis), n.d. not detected. Inhibitor experiments with GSK2033 were carried out as follows: In the GSK 2033 treated groups, cells were pretreated with GSK 2033 (5 µM) for 2 hours before SH42 treatment. Cells were ultimately incubated with SH42 (5 µM). RNA was isolated using Tripure RNA Isolation reagent (Roche) according to the manufacturer's protocol. Total RNA (1 µg) was reverse transcribed using Moloney Murine Leukemia Virus (M-MLV) Reverse Transcriptase (Promega) for RT-qPCR according to the manufacturer's instructions to produce cDNA. mRNA expressions were normalized to β-actin and Cyclophilin A mRNA expressions and expressed as fold change compared to vehicle-treated groups using the ΔΔCT method. Primer sequences can be found in **supplementary material S11**. For further details please refer to the materials and methods section.

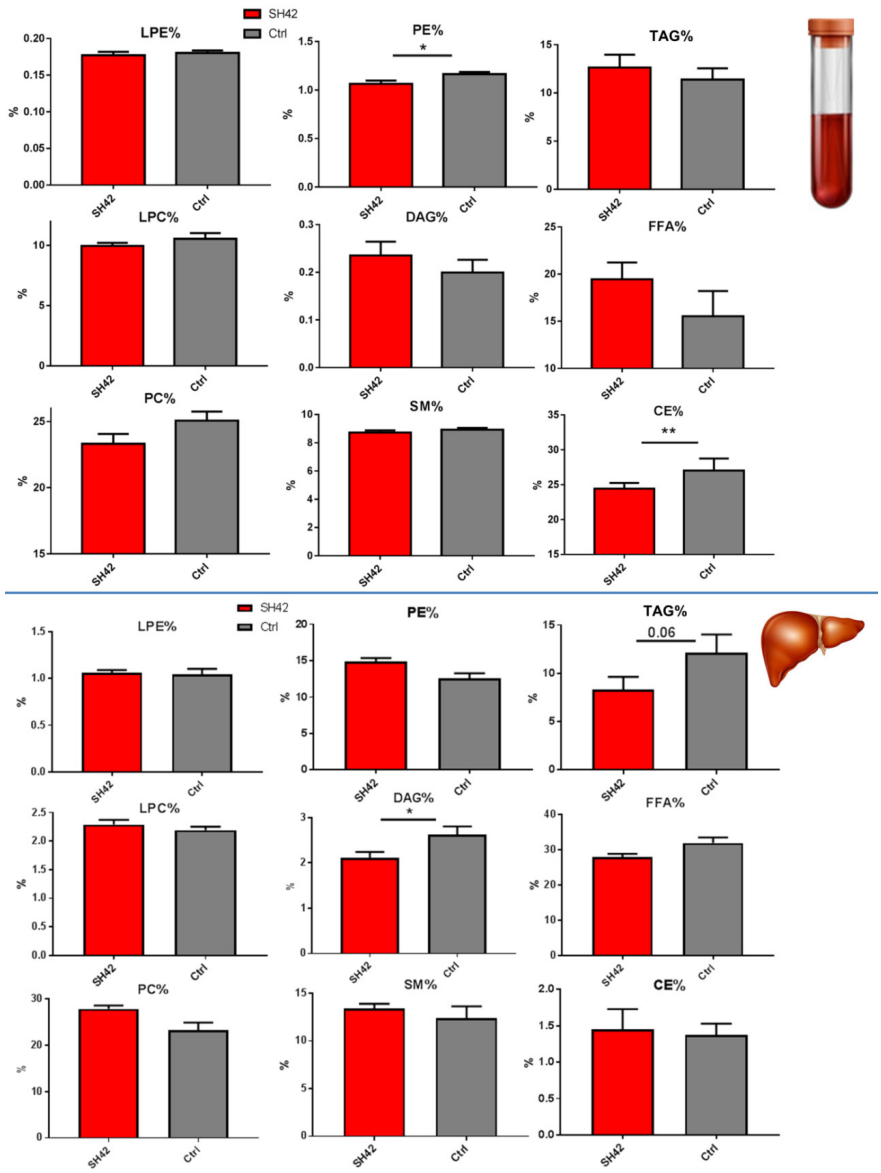

S3. Serum (above) and liver (below) lipid class composition obtained after three day treatment with 0.5 mg/d SH42 versus vehicle control (Ctrl). All experiments n=5, mean±SEM, non-parametric students t-test (Mann-Whitney), * $p<0.05$, ** $p<0.01$. LPE lysophosphatidylethanolamine, LPC lysophosphatidylcholine, PC phospatidylcholine, PE phospatidylethanolamine, DAG diacylglycerolm SM sphingomyeloid, TA triacylglyceride, FFA free fatty acid, CE cholesteryl ester. Lipid compositional analysis for the aforementioned lipid classes is shown. Lipidomics analysis was carried out as described in **supplementary material S15.**

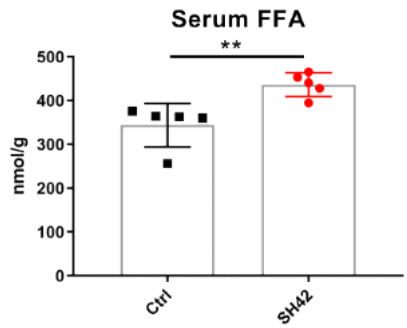

S4. Serum free fatty acid (FFA) concentration, ** p<0.01, mean±SEM, non-parametric students t-test (Mann-Whitney) n=5, FFA = free fatty acids. The serum FFA concentration as obtained by quantitative lipidomics analysis (**supplementarymaterial S15**) is shown. The absolute concentration of the FFA lipid class is shown as nmol/g serum.

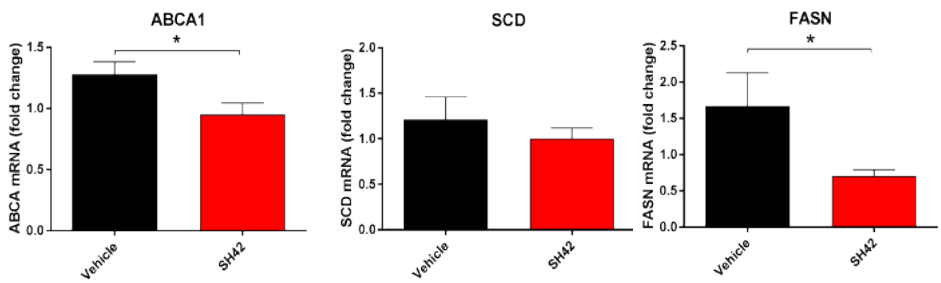

S5. qPCR analysis of liver genes comparing vehicle and 3 day SH42 treatment. All experiments n=5. non-parametric students t-test (Mann-Whitney), mean±SEM, * p<0.05.

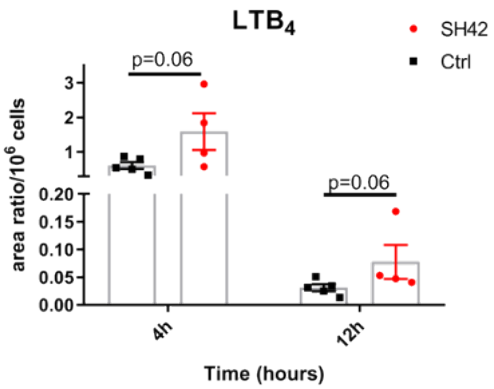

S6. LTB_4 analysis, non-parametric students t-test (Mann-Whitney), mean±SEM, n=4-5. LTB_4 was assessed using LC-MS analysis as described in **supplementary material S16**. Mice were sacrificed 4 and 12 hours after zyA injection with and without SH42 treatment (0.5mg for 3 days). Area ratios corrected for the internal standard d4-LTB_4 and cell numbers are given.

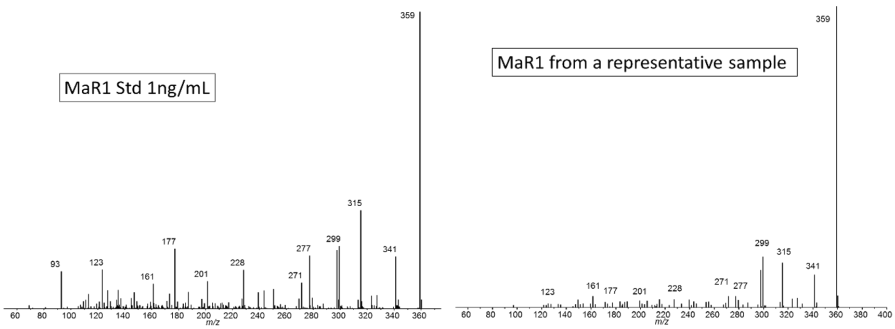

S7. Tandem MS spectra for MaR1 in comparison to authentic standard material.

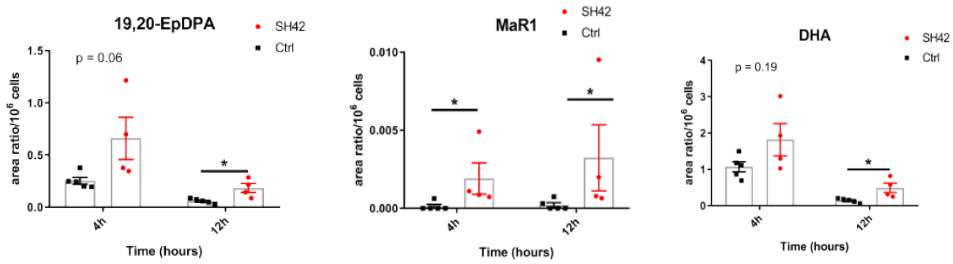

S8. Validation experiment for DHA, MaR1 and 19,20-EpDPA, non-parametric students t-test (Mann-Whitney), one per time point, mean±SEM, n=4-5, * p<0.05. Lipids were assessed using LC-MS analysis as described in **supplementary material S16**. Mice were sacrificed 4 and 12 hours after zyA injection with and without SH42 treatment. Area ratios corrected for the internal standards d4-LTB_4 (19,29-EpDPA and MaR1) or d5-DHA (DHA) and cell numbers are given.

S9. Procedures used for cell shape analysis. Cell shape analysis has become an accepted parameter differentiating M1 and M2 MΦs [1]. Image analysis was carried out as described elsewhere [2] and lined out below. The cell morphology was analyzed by phase contrast images and measurements of the cell shape, cell length and perimeter in each high-power field (magnification ×200).

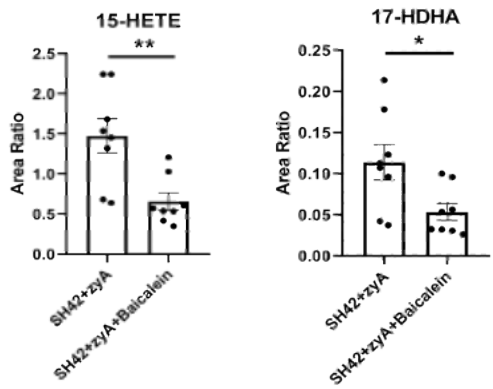

S10. Baicalein blocks the SH42 induced accumulation of the 15-LOX pathway markers 15-HETE and 17-HDHA. M1 macrophages (5×10^6 cells) were treated with zyA and SH42 with and without 1 µg/mL Baicalein for 24 hours. N=8, mean±SEM, (4 biological (donors) and 2 technical repeats). Non parametric students t-test (Mann-Whitney), * p<0.05, ** p<0.01. 15-HETE and 17-HDHA were assessed using LC-MS analysis as described in **supplementary material S16**. Area ratios corrected for the internal standard d8-15-HETE are shown.

S11. Primer sequences

LXR and LXR selectivity assessment

Transcription factor	Gene	Forward Primer Sequence (5'-3')	Reverse Primer Sequence (5'-3')
LXR	*Abca1*	CCCAGAGCAAAAAGCGACTC	GGTCATCATCACTTTGGTCCTTG
LXR	Abcg1	AGGTCTCAGCCTTCTA-AAGTTCCTC	TCTCTCGAAGTGAAT-GAAATTTATCG
	β-actin	AACCGTGAAAAGATGAC-CCAGAT	CACAGCCTGGATGGCTACGTA
	Cyclophilin A	ACTGAATGGCTGGATGGCAA	TGTCCACAGTCGGAAATGGT
PXR	*Cyp3a11*	CACAAACCGGAGGCCTTTTG	ATCCATGCTGTAGGCCCCAA
PXR; FXR	*Cyp7a1*	CAGGGAGATGCTCTGTGTTCA	AGGCATACATCCCTTCCGTGA
PXR; RXR	*Cyp27a1*	TCTGGCTACCTGCACTTCCT	CTGGATCTCTGGGCTCTTTG
FXR	*Shg*	TCTGCAGGTCGTCCGACTATT	TGTCTTGGCTAGGACATCCA
LXR	*Srebp1c*	AGCCGTGGTGAGAAGCGCAC	ACACCAGGTCCTTCAGT-GATTTGCT

Abca1, ATP-binding cassette sub-family A member 1; *Abcg1*, ATP-binding cassette sub-family G member 1; *Srebp1c*, sterol regulatory element-binding protein 1 isoform c, *Cyp, cytochrome P.*

Peritoneal cell analysis

Gene	Forward Primer Sequence (5'-3')	Reverse Primer Sequence (5'-3')
18S	GTAACCCGTTGAACCCCATT	CCATCCAATCGGTAGTAGCG
SCD-1	TCGGGATTTTCTACTACATGACCA	ACGTCATTCTGGAACGCCA
Elovl1	GCCTCGAATCATGGCTAATC	CCTTGGAAAGCATGAAGAGC
Elovl5	ATGGACACCTTTTTCTTCATCCTT	ATGGTAGCGTGGTGGTAGACATG
Elovl6	TCGAACTGGTGCTTACATGC	GAGCACAGTGATGTGGTGGT
Fads6	CAGCACATCGGACTGCCTAT	ACACCAAGGGCTTCACCTTC

SCD-1, Stearoyl-CoA desaturase-1*; Elovl1, 5, 6* Elongation of very long chain fatty acids protein 1, 5, 6; *Fads6,* fatty acid desaturase 6

Macrophage phenotype determination (human)

Gene	Forward Primer Sequence (5'-3')	Reverse Primer Sequence (5'-3')
ALX/FPR2	TGT TCT GCG GAT CCT CCC ATT	CTC CCA TGG CCA TGG AGA CA
Arg1	TGG ACA GAC TAG GAA TTG GCA	CCA GTC CGT CAA CAT CAA AAC T
BAI1	AGC CAC TGA CAT CAG CTT CC	ATG CTT CAT CGG CCT CTG TC
CD36	CTTGGCTTAATGAGACTGGGAC	GCA ACA AAC ATC ACC ACA CCA
CD80	AGC CTC ACC TCT CCT GGT TG	TGG GGC AAA GCA GTA GGT CA
CD163	ACA ACA GGT CGC TCA TCC C	GTG TGG CTC AGA ATG GCC T
CD206	CCC TCA GAA AGT GAT GTG CCT	TCT CCA CGA AGC CAT TTG GT
ChemR23	AGG GAC TGA TTG GCT GAG GA	ATC CTC CAT TCT CAT TCA CCG T
CX3CR1	AAT GCC TGG CTG TCC TGT GT	GCC TGC TCC TTT GTG ATT CAG
GPR18	ACA GAA GTG GAA GTG CTG AAA A	CAG AAA GCA GCA CCT CCT GT
GPR32	GGG CCT GCA AAC TCT ACA	GGA GGC AGT TAC TGG CAA
IL-6	CAC CAG GCA AGT CTC CTC AT	GAC AGC CAC TCA CCT CTT CA
IL-10	AAT CGA TGA CAG CGC CGT AG	GGT TGC CAA GCC TTG TCT GA
STAT-1	ATC AGG CTC AGT CGG GGA ATA	TGG TCT CGT GTT CTC TGT TCT
TIM4	ACA GGA CAG ATG GAT GGA ATA CCC	AGC CTT GTG TGT TTC TGC G

FPR2, N-formyl peptide receptor 2; *Arg1*, Arginase 1; *STAT-1*, Signal transducer and activator of transcription 1; *TIM4,* T-cell immunoglobulin mucin protein 4.

S12. GC-MS analysis.

We used a Bruker Scion GC/MS system, operated in scan mode from *m/z* 100-550. Helium 99.9990% was used as carrier gas at a constant flow rate of 1.4 mL/min. Injector and transfer line were operated at 280 °C. The oven program started at 90 °C held for 0.5 minute, then ramped to 270 °C at 30 °C/minute, ramped to 310 °C at 10 °C/minute. The following masses were used to quantify desmosterol levels against an external calibration line (0 – 10 ppm) *m/z* 445 + 355 for cholestanol (IS), *m/z* 357 and 271 for cholestan (IS) and *m/z* 343 + 253 for desmosterol.

Serum desmosterol levels were determined as described elsewhere [3]. Liver desmosterol levels, were monitored as follows: livers samples were homogenized in a bullet blender after the addition of 500 µL LC-MS grade water for 2 min. To 100 µL of the homogenate was added 100 µL 10M NaOH and 10 µL of a cholestanol solution (100 µg/mL, serving as internal standard). The sample was hydrolysed for 30 minutes at 60°C. After the addition of 100 µL LC-MS grade water, lipids were extracted with 500 µL methyl-*tert*-butyl ether (MTBE). The organic extract was dried under a gentle stream of nitrogen and 29 µL MTBE, 20 µL MSTFA and 1 µL pyridine were added. After storing the sample for 30 minutes at room temperature, 1 µL was injected splitless. In the case of peritoneal cell desmosterol levels, cells were pelleted and washed once with PBS. The cell pellet was resuspended in 250 µL 2-propanol and washed into a glass vial. The tube was subsequently washed with another portion of 250 µL 2-propanol and the organic solvent was combined. After drying under a gentle stream of nitrogen 100 µL water and 50 µL 10 M NaOH and 10 µL cholestan solution (100 µg/

mL, serving as internal standard) (cholestanol in the case of macrophages) were added to the lavage cells and hydrolysis was accomplished for 30 min at 60°C, lipids were extracted twice with 500 µL methyl-tert.-butyl ether (MTBE). The organic extract was dried under a gentle stream of nitrogen and 79 µL MTBE, 20 µL MSTFA and 1 µL pyridine were added. After storing the sample for 30 minutes at room temperature, 1 µL was injected splitless. For whole blood analysis after 1 or 2 days of SH42 treatment, 50 µL whole blood was spiked with 10 µL cholestan solution and 25 µL 10M NaOH and 100 µL water for hydrolyisis were added. Extraction and derivatization were carried out as described for the lavage cells. For all experiments a freshly prepared calibration line with authentic desmosterol (0-10 ppm) was prepared on the day of analysis.

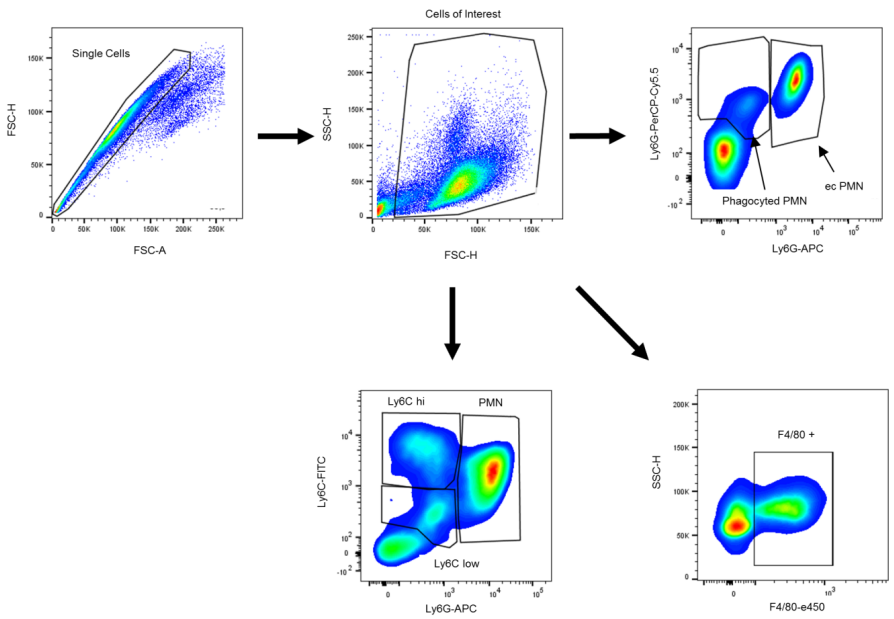

S13. Representative figure of the FACS gating strategy for leukocyte differentiation and efferocytosis. Leukocytes were gated on FSC/SSC. Leukocyte subtypes were further classified into Ly6G^{hi} Ly6C^{hi} and Ly6C^{lo}. For defining efferocytosis the differentiation of intra and extracellular PMN was assessed by using Ly6G-PerCP-Cy 5.5 and Ly6GAPC antibodies. Phagocytized PMNs were Ly6G-PerCP-Cy5.5 positive and Ly6G APC negative.

S14. Protein array analysis

Average signal intensity of 6 replicates was normalized to the median signal of all antibodies on the array. The presented fold change represents the ratio of the normalized signal from SH42 treated mice compared with vehicle treated controls. GAPDH and beta actin were used as housekeeping proteins. Data analysis was performed with IPA software (Qiagen). Pathways were substantiated and updated with recent literature.

S15. Quantitative lipidomics analysis

Briefly: for liver samples, one liver lob was homogenized in an Eppendorf tube with 600 µL LCMS grade water and pre-washed stainless steel beads. An aliquot corresponding to approximately 2 mg liver tissue was worked up. For serum samples, 100 µL was worked up. To the samples in 2 mL Eppendorf tubes was added 100 µL internal standard mix (Lipidyzer kit) in MTBE. Subsequently 500 µL MTBE and 160 µL methanol were added, the mixture was shaken for 30 minutes at room temperature, before 200 µL of water was added. The samples were spun at 16,100 ×g for 3 minutes and the upper organic layer transferred to a glass vial. The remaining sample was extracted again by the addition of 300 µL MTBE, 100 µL methanol and 100 µL for 30 minutes. After centrifugation the organic extracts were combined and dried under a gentle stream of nitrogen. The dry extract was dissolved in 250 µL Lipidyzer running buffer and analysed according to the manufacturers protocol (4, 5). For data analysis the Excel spread sheets were transformed into comma separated files (.csv). FA composition analysis calculates the total of a given FA within a class divided by the total of all the FA within that class. In this way a FA fractional analysis for each class of analysed lipids has been carried out. For further analysis volcano plots were built in order to visualize the different FA compositions of liver, serum and peritoneal cells. For this, missing values in each dataset were imputed with half of the minimum concentration value and all determined fractional values were centred around the mean value of each analyte. For the volcano plot we set the fold change threshold to 1.5 and the p-value threshold to 5%, and the control group was considered as the reference in all comparisons.

S16. Targeted lipid mediator analysis

Peritoneal lavage samples were spiked with 4 µL of an internal standard solution (containing d4-PGE4, d4-LTB4 d8-15-HETE and d5-DHA at a concentration of 50 ng/ml (500ng/mL for d5-DHA) in methanol). The samples were transferred to a 12-ml glass vial, and 1.75 ml of methanol was added. The samples were centrifuged at 4,000 rpm for 5 min at 6 °C, and the supernatant was transferred to a fresh 12-ml glass vial. The pellet was re-extracted with 500 µl of methanol and centrifuged as described above, and the organic extracts were combined. The methanol was partially removed under a gentle stream of nitrogen at 40 °C for 30 min. The remaining methanolic extract (approximately 1.5 ml) was diluted with 8 mL of water, and 10 µL of 6 M HCl was added. The prepared samples were cleaned via solid phase extraction (SPE) (SepPak C18 200 mg, Waters, MA, USA). The samples were loaded onto preconditioned SPE cartridges (2 ml methanol, followed by 2 ml water), the cartridges were washed with 3 ml of water followed by 3 ml of n-hexane, and then the samples were eluted with 3 ml of methylformate. The eluate was dried under a gentle stream of nitrogen, reconstituted in 200 µL of 40% methanol, and injected.

LC-MS/MS analysis was performed as described below. Briefly, a QTrap 6500 mass spectrometer operating in negative ESI mode (Sciex, Nieuwerkerk aan den Ijssel, The Netherlands) was coupled to an LC system employing two LC-30AD pumps, a SIL-30AC autosampler, and a CTO-20AC column oven (Shimadzu,'s-Hertogenbosch, The Netherlands). A 1.7 µm Kinetex C18 50 × 2.1 mm column protected with a C8 precolumn (Phenomenex, Utrecht, The Netherlands) was used, and the column was maintained at 50 °C. A binary gradient of water (A) and MeOH (B) containing 0.01% acetic acid was generated as follows: 0 min 30% B, held for 1 min, then ramped to 45% B at 1.1 min, 53.5% B at 2 min, 55.5% B at 4 min, 90% B at 7 min, and 100% B at 7.1 min, and held for 1.9 min. The injection volume was 40 µl, and the flow rate was 400 µL/min. For analyte identification, the mass transition used

for each analyte was combined with its relative retention time (RRT). The calibration lines constructed with standard material for each analyte were used for quantification, and only peaks with a signal to noise (S/N) ratio > 10 were quantified

In the case of treated M1 MΦ, quenched cells in 1.5 mL methanol were spun for 5 min at 4000 ×g and the supernatant transferred to a 1.5 mL glass vial. After spiking samples to a final concentration of 1 ng/mL (d4-PGE2, d4-LTB4 and d8-15HETE) and 10 ng/mL (d5-DHA) with internal standards, samples were dried under a gentle stream of nitrogen, resuspended in 150 µL 40% methanol, spun again for 3 min at 18.000 ×g and transferred to micro vial inserts for LC-MS/MS analysis.

Supplemental references

1. Korner, A., et al., *Sympathetic nervous system controls resolution of inflammation via regulation of repulsive guidance molecule A.* Nat Commun, 2019. **10**(1): p. 633.
2. McWhorter, F.Y., et al., *Modulation of macrophage phenotype by cell shape.* Proc Natl Acad Sci U S A, 2013. **110**(43): p. 17253-8.
3. Muller, C., et al., *New chemotype of selective and potent inhibitors of human delta 24-dehydrocholesterol reductase.* Eur J Med Chem, 2017. **140**: p. 305-320.